# FLUTTER CONTROL OF WING BOXES USING PIEZOELECTRIC ACTUATORS

A Thesis
Submitted to the Faculty
of
Purdue University
by
Edwin Ewald Forster

In Partial Fulfillment of the
Requirements for the Degree
of
Master of Science in Aeronautics and Astronautics
August 1994

# ACKNOWLEDGMENTS

I would like to thank Professor Henry T. Y. Yang for the help he has given me, especially the sharing of his insight of physical structures. I would also acknowledge the United States Air Force Palace Knight Program which has given me the opportunity to continue my education. I would like to express my appreciation to Professors Terrence Weisshaar and Martin Corless for being on my graduate committee and always finding time to lend help. Also, I am very grateful for the suggestions and guidance given by Dr. Vipperla B. Venkayya, who has been my mentor in the Palace Knight Program . Lastly, I would like to thank my friends and family who have supported me throughout this experience.

TABLE OF CONTENTS

# LIST OF TABLES

# LIST OF FIGURES

Figure Page

# ABSTRACT

Forster, Edwin Ewald. M.S.A.A., Purdue University, August 1994. Flutter Control of Wing Boxes Using Piezoelectric Actuators. Major Professor: Henry T. Y. Yang.

This paper examines the use of piezoelectric actuators to control supersonic flutter of wing boxes. Aluminum built-up wing boxes are used as examples to analyze the free vibration, aeroelastic, and control concepts associated with flutter control. Finite elements are used to calculate deflections due to input forces, the member stresses and strains, natural frequencies, and mode shapes. Linear strip theory with steady aerodynamics are applied to find the frequency coalescence of modes indicating flutter. The variables of interest are the skin, web, and rib thicknesses associated with torsional rigidity, and the spar cap and vertical post areas associated with bending rigidity. Piezoelectric actuators are implemented in a configuration which generates torsional control of the wing box. Pole assignment concepts are applied to change the free vibration frequencies. A parametric study changing the free vibration frequencies using piezoelectric actuators is conducted to determine which thicknesses of skins, webs, and ribs will meet a specified flutter requirement. The addition of piezoelectric actuators will allow the flutter requirements to be met at smaller thicknesses of skins, webs, and ribs so that the overall weight of the wing box, including actuators, is decreased.

# CHAPTER 1

# INTRODUCTION

Flutter is defined as the instability associated with increasing amplitude of oscillations due to the interaction of modes with inertial and aerodynamic coupling. This aeroelastic instability is a concern of aircraft and wing designers. Traditionally, control of this instability has been primarily accomplished using conventional lift control surfaces such as ailerons. More recently, advanced control devices such as strain actuators have been proposed to control flutter.

## Flutter Suppression

Active flutter suppression uses control surfaces with classic control techniques to change the aeroelastic behavior of a wing. The field of aeroservoelasticity has been explored by many investigators, such as Zeiler and Weisshaar[1], and Karpel[2]. Zeiler and Weisshaar[1] presented the problem of integrated aeroservoelastic tailoring using a four degree of freedom aeroelastic model. Karpel[2] analytically developed the flutter and stability margin derivatives with respect to aeroservoelastic design. A mathematical model of the Active Flexible Wing (AFW) wind tunnel model is used for a numerical example. Among those who summarized the works on aeroservoelasticity, Noll[3] described the work of the Aeroservoelasticity Branch of the NASA Langley Research Center on the Active Flexible Wing program. Wind tunnel tests on the AFW have reported a 20% increase in flutter dynamic pressure

## Active Structures

Structural control approaches were proposed by Wada, Fanson, and Crawley[4] to include sensing structures and adaptive structures as the two most basic categories. Sensory structures possess sensors for the determination of the system states and characteristics. Adaptive structures possess actuators to change the system states and characteristics. Wada, Fanson, and Crawley[4] stated that active structures incorporate sensory and adaptive structures such that the "distinction between control functionality and structural functionality are blurred." Active vibration damping and shape control of space structures using shape memory alloy was an example among those given by Stevens[5]. Another example supplied by Stevens[6] was the use of magnetostrictive alloy to optimize the performance of a wing under changing flight conditions. An overview of the recent developments in active structures was reported by Wada[7], using the abstracts submitted to the 30th SDM Conference. The focus on using active truss-type structures for future space structures was evidenced by the variable geometry and adaptive planar truss. These structures were described as responsive to space assembly and deployment.

## Piezoelectric Actuators

An adaptive material which has the property of piezoelectricity is suited for control applications beyond 1 KHz. A piezoelectric material produces an electric field when stress or strain is applied. Conversely, these materials can produce a stress, and therefore a strain, when an electric field is applied. Examples of piezoelectrics include lead zirconate titanate (PZT) and polyvinylidine fluoride (PVDF). Because of their dual nature, piezoelectrics can both act as sensors and actuators. Jaffe[8] proposed that the discovery of the poling process was a significant step to understanding piezoelectricity in ceramics. Poling is the "application of a high voltage sufficient to reverse electric moments of spontaneously polarized regions in the ceramic." Mason[9] indicated that early uses of

piezoelectrics included acoustic wave devices, ultrasonic experiments, and wave filters. Recently, they have been used in experiments involving damping of vibrations.

Barrett[10] explored different piezoelectric configurations to produce torque on a plate. Examples showed that directionally attaching an inplane orthotropic actuator restricted longitudinal displacements while the lateral displacements had little restriction. With this method, a host structure consisting of an isotropic material could be twisted using a piezoceramic, such as PZT. Abdul-Wahed and Weisshaar[11] created a three-dimensional isoparametric solid finite element to model an adaptive material. Examples included cantilever beams with a skewed PZT actuator array which produced deflection and twist, and skewed axis PVDF actuator arrays which created twist only. Experimental control of a composite slender beam with embedded piezoelectric actuators was the focus of de Luis and Crawley[12]. These experiments concluded that the control of flexible modes could be accomplished using piezoelectric actuators. Ehlers and Weisshaar[13] examined the use of piezoelectrics to enhance static aeroelastic behavior of composite wings. Lazarus, Crawley, and Bohlmann[14] examined the feasibility of using adaptive materials for static aeroelastic control of a box wing. Twist was generated through bending/twist coupling and extension/twist coupling. The trade studies performed showed that better control authority with decreased weight could be obtained for some wing configurations. Lazarus, Crawley and Lin[15] conducted a typical section analysis to determine the effectiveness of torsion and bending strain actuation verses leading and trailing edge flap control. Control cost comparisons indicated that for the two degree of freedom section, one bending and one torsion actuator produce the best combination.

## Scope

In this paper, the analysis of feasibility of flutter control of a fully built-up wing box with piezoelectric actuators is presented. The natural frequencies and mode shapes

are computed using the finite element program by Venkayya and Tischler[16]. The program uses a Sturm sequence to solve the free vibration problem. Adequate validation of the program's capabilities are addressed by the mapping of mode shapes of the wing box and comparison of natural frequencies with previously published data[17]. The aerodynamic forces are obtained from two-dimensional linear strip theory. Steady aerodynamics are used so that flutter would be indicated by the coalescence of modes. The first three modes are used to reduce the order of equations of motion. These modes correspond to first bending, first torsion, and second bending. The aerodynamic and flutter model are verified by comparison with the three bay model analyzed by Striz and Venkayya[17], and Rudisill and Bhatia[18,19]. The divergence speed of the six bay model is checked with Bowman, Grandhi, and Eastep[20]. These comparisons are all in the subsonic regime; however, the only changes in the aerodynamic model for the supersonic regime occur in the relocation of the aerodynamic center from the quarter chord to the half chord, and changing the lift curve slope. Flutter predictions in the supersonic regime associated with frequency crossing and mode switching are presented. A piezoelectric actuator configuration which controls the twist of the wing box is implemented to change the free vibration frequencies and thus it controls the flutter speed. An important contribution is the parametric study which determines the thicknesses of skins, webs, and ribs that meet a specified flutter requirement for piezoelectric actuator control of the free vibration frequencies. The weight of the wing box can be decreased by adding piezoelectric actuators to meet the flutter requirement at smaller thicknesses of skins, webs, and ribs.

# CHAPTER 2

# MODEL CONFIGURATION

To facilitate the study of the control of flutter using induced strain actuators, representative models of the wing structure, aerodynamics, and piezoelectric actuators are constructed. Simple models that characterize the system behavior are desirable to lessen computational burdens. Membrane and rod finite elements formulate a wing box, linear strip theory models the aerodynamics, and a rod finite element is used to model the induced displacements created by a piezoelectric actuator.

## Finite Element Model

An example of the wing box is depicted in Figure 1. It is assumed to be a six bay model. The skins are modeled using twelve 8-d.o.f. quadrilateral membrane elements. The webs and ribs are modeled using eighteen 8-d.o.f. shear panel elements, and the spar caps and vertical posts are modeled using thirty-six 2-d.o.f. bar elements. The finite element formulations are based on those presented by Venkayya and Tischler[16]. The quadrilateral membrane element stiffness is determined by breaking it into four component triangular membrane elements. The fifth fictitious node is removed by static condensation. The shear panels are constructed similarly to the quadrilateral membrane element but with the stiffness matrices determined by considering only the shear strain energy. The structure behaves similarly to idealized wing boxes in Megson[21] in which the stringers carry direct stress and the skins and webs carry shear stresses.

The six bay wing box is the same model used by Bowman, Grandhi, and Eastep[20], which is a modified version of the three bay wing box optimized for flutter by Rudisill and Bhatia[18,19]. Striz and Venkayya[17] stated that the use of membrane elements for webs and ribs over predict the stiffness of a wing. The aspect ratio of 15 for the webs was too high, even for dynamic analysis. Striz and Venkayya demonstrated this understanding using the wing of Rudisill and Bhatia.

The finite element variables of thickness and cross sectional area are assumed to be uniform over the span of the wing box. Furthermore, the skin, web, and rib members, which are associated with torsional rigidity, are assumed to have the same thicknesses and the spar cap and vertical post members, which are associated with bending rigidity, are assumed to have the same cross sectional areas. The symmetry of the wing box always locates the shear center in the center of the wing box. The uniform wing without non-structural masses has the center of mass at the same location as the shear center. The addition of non-structural mass, say, equal to the structural mass along the rear spar, will locate the center of mass midway between the rear spar and the shear web.

## Aerodynamic Model

The location of the wing box in the aerodynamic shell is shown in Figure 2. The shell is assumed to not carry any structural stresses and all aerodynamic forces are directly translated to the spars. For subsonic and supersonic flight the aerodynamic center (A.C.) is assumed to be located at the quarter chord and the half chord, respectively. For subsonic flow the aerodynamic center is in front of the shear center (S.C.), whereas for supersonic flow the aerodynamic center is aft of the shear center.

The two-dimensional aerodynamic grid is attached to the structure with six aerodynamic strips: the edges are lined up with the ribs of the structure. The ribs and aerodynamic strips are assumed to stay perpendicular to the span as the wing is swept.

The aerodynamic loads acting on a strip are assumed to be functions of the deflections of only that strip. The lift is given as

$$L = \frac{1}{2} \rho V_n^2 S C_{L_\alpha} \alpha_{eff} \tag{1}$$

where $V_n$ is the chordwise component of the actual airspeed. The air density, $\rho$, is dependent on the altitude, and the lift curve slope, $C_{L_\alpha}$, is dependent on Mach number. The effective angle of attack is the angle of the strip with respect to $V_n$

$$\alpha_{eff} = \alpha - \Gamma \tan \Lambda \tag{2}$$

where $\alpha$ is the chordwise rotation, $\Gamma$ is the spanwise rotation, and $\Lambda$ is the sweep of the section with respect to the free stream.

## Piezoelectric Actuator Model

A piezoelectric material produces a three dimensional state of strain when an electric field is applied. For the case of stress free expansion, the relation between strains and electric fields is

$$\begin{Bmatrix} \varepsilon_{11} \\ \varepsilon_{22} \\ \varepsilon_{33} \\ \varepsilon_{23} \\ \varepsilon_{31} \\ \varepsilon_{12} \end{Bmatrix} = \begin{bmatrix} & & -d_{31} \\ & & -d_{32} \\ & & -d_{33} \\ & -d_{24} & \\ -d_{15} & & \end{bmatrix} \begin{Bmatrix} E_1 \\ E_2 \\ E_3 \end{Bmatrix} \tag{3}$$

where $\{\varepsilon\}$ is the vector of strains, [d] is the matrix of piezoelectric charge coefficients and $\{E\}$ is the vector of applied electric fields. PZT is an inplane orthotropic material. PVDF is an isotropic material with orthotropic electrically induced inplane strains. The magnitude of the charge coefficient directly relates the amount of unrestricted strain that can be achieved for a particular direction. The charge coefficients of PVDF are larger

than those of PZT. For a piezoceramic, such as PZT, the shear charge coefficients ($d_{24}$,$d_{25}$) are the largest, the charge coefficient in the poling direction ($d_{33}$) is second largest, and the charge coefficients in the plane perpendicular to the poling direction ($d_{31}$,$d_{32}$) are the smallest in magnitude. Most current applications utilize this last type of configuration.

A comparison of material properties of aluminum and piezoelectric materials appears in Table 1. PZT has the approximate modulus of aluminum with the density of steel which makes it a potentially good actuator. PVDF has a much smaller modulus and so it is more suitable for a sensing medium. PZT has the inherent problem of brittleness related to all ceramics. Carter[22] relates that sheets are available in 0.005", 0.0075", and 0.010" thicknesses. For the nominal thickness of 0.0075", the maximum voltage applied is 40-50 volts in the poling direction, relating to a maximum strain of approximately 300 $\mu\varepsilon$.

In this study a standard axial force member is used to model the piezoelectric actuator. The actuator configuration is shown in Figure 3. The arrows indicate the resultant force on the wing box due to activation of the piezoelectric actuators. The piezoelectric actuator under compression pushes the host structure outward, the actuator in tension is pulling the host structure inward. The upper and lower skins each have an actuator in compression and in tension for a positive electric field. A negative electric field reverses the actions of the members. Twisting of the wing box is caused by shearing the upper and lower skins in opposite directions. The lateral strain of the piezoelectric actuators is ignored because the actuators are assumed directional. Axial force members are used because of the high aspect ratio of the actuator elements. All strips are assumed to be 1" wide with height equal to the number of layers multiplied by the nominal thickness 0.005". Buckling of such long, thin members is neglected because the elements are assumed to be bonded to the skin surface. For PZT actuators, this simplification of the

actuator attachment follows Barrett's[10] work to directionally attach PZT elements to host structures.

The axial force member will produce a strain dependent on the electrical and mechanical loading

$$\varepsilon = \varepsilon^{M} + \varepsilon^{E} \tag{4}$$

where the superscript M indicates mechanical and the superscript E indicates electrical. The finite element method uses a simple superposition of electrical forces and forces in the member due to the induced displacements to find the resultant force in the member, as outlined by Yang[23].

Table 1. Comparison of material properties of aluminum and piezoelectric materials.

| Material Properties | Aluminum | PZT | PVDF |
|---|---|---|---|
| Modulus ($10^6$ psi) | 10.0 | 9.135 | 0.29 |
| Density (lb/in$^3$) | 0.1 | 0.275 | 0.064 |
| Poisson's Ratio | 0.3 | 0.35 | 0.3 |
| Tensile Strength (ksi) | 65.0 | 9.135 | 4.5-8.0 |
| Compressive Strength (ksi) | 65.0 | 75.4 | --- |

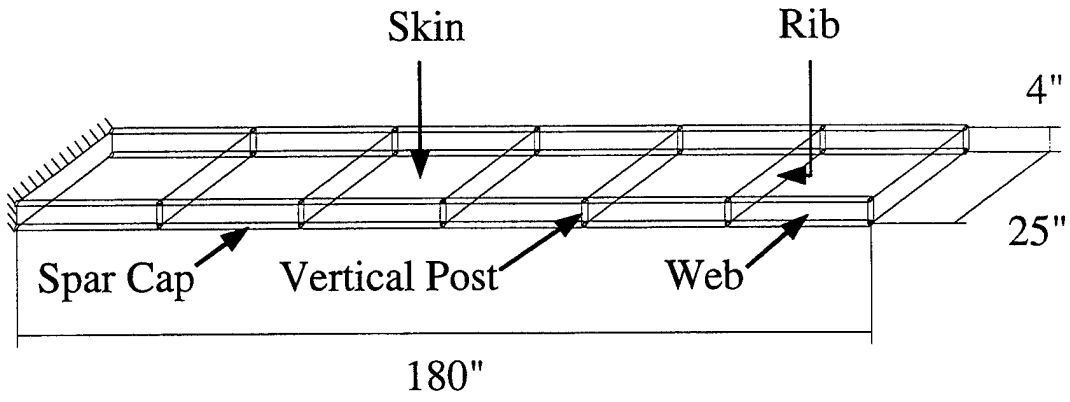


Figure 1. Dimensions and member identification of the built-up aluminum wing box.

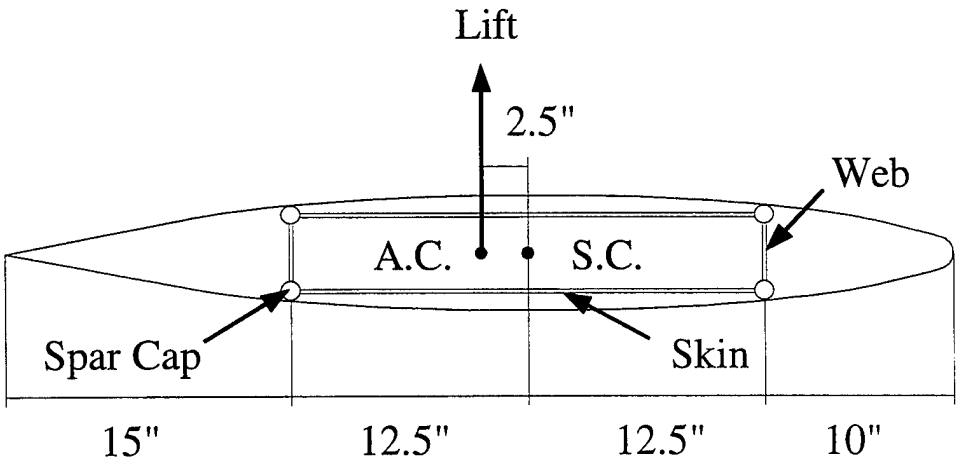


Figure 2. Cross section of wing.

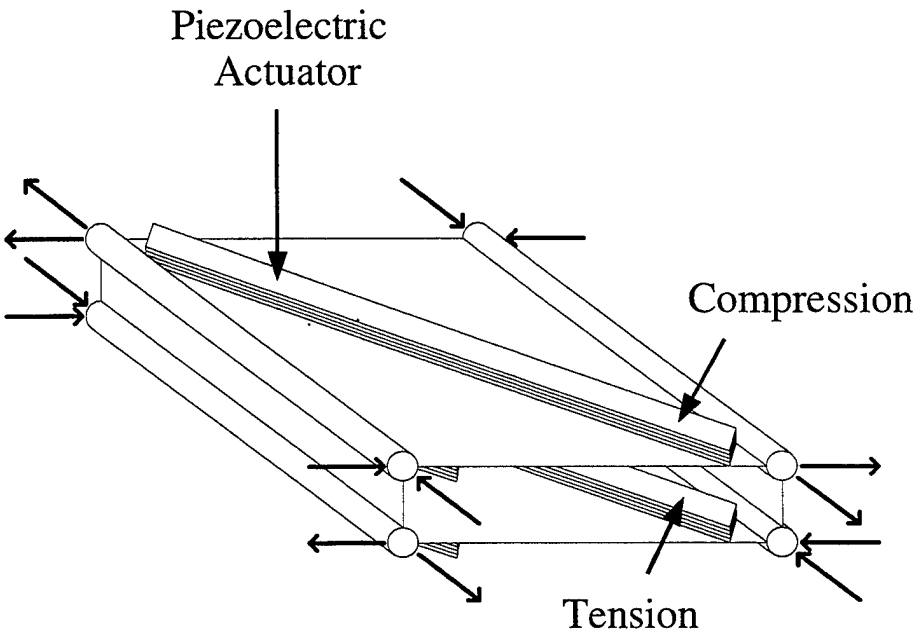


Figure 3. Piezoelectric actuator configuration.

# CHAPTER 3

# STRUCTURAL DYNAMICS AND CONTROL ANALYSIS

The equations of motion are formulated to analyze the free vibration, flutter, and control characteristics of the system. The equations are constructed for the general analyses of finding the natural frequencies and mode shapes, frequency coalescence indicating flutter, and assignment of the system poles.

## Free Vibration Analysis

The equations of motion for the wing box is

$$[M]\{\ddot{X}\} + [K]\{X\} = \{F(t)\} \tag{5}$$

where $[M]$ is the mass matrix, $[K]$ is the stiffness matrix, $\{X\}$ is the vector of nodal displacements, $\{\ddot{X}\}$ is the vector of nodal accelerations, and $\{F(t)\}$ is the vector of forcing functions. The mass matrix is assembled using lumped mass formulation for membrane, shear panel, and bar elements. For the case of free vibration, the problem becomes an eigenvalue problem

$$\left[[K] - \omega^2[M]\right]\{U\} = \{0\} \tag{6}$$

where $\omega$ is the natural frequency, and $\{U\}$ is the mode shape.

Defining a new vector $\{\eta\}$ as the orthonormal mode

$$\left\{\eta^{(k)}\right\} = \frac{1}{\sqrt{M_{kk}}}\left\{U^{(k)}\right\} \tag{7}$$

where

$$M_{kk} = \left\{U^{(k)}\right\}^T[M]\left\{U^{(k)}\right\} \tag{8}$$

The equations of motion can simplified using the information of the free vibration natural frequencies and mode shapes.

## Aeroelastic Analysis

In the case of steady aerodynamics, the vector of forcing functions is replaced by

$$\{F(t)\} = [A]\{X\} \tag{9}$$

where [A] is the matrix of aerodynamic influence coefficients.

By substituting into the equation

$$\{X\} = [\Phi]\{Q\} \tag{10}$$

where $[\Phi]$ is the matrix of orthonormal modes, and premultiplying the equation by $[\Phi]^T$, the equations of motion become

$$[\Phi]^T[M][\Phi]\{\ddot{Q}\} + [\Phi]^T[K][\Phi]\{Q\} = [\Phi]^T[A][\Phi]\{Q\} \tag{11}$$

This equation is simplified by substituting back the relations for orthonormal modes

$$[I]\{\ddot{Q}\} + \left[\Omega^2\right]\{Q\} = [\Phi]^T[A][\Phi]\{Q\} \tag{12}$$

where $\left[\Omega^2\right]$ is the diagonal matrix of natural frequencies. This equation can then be put into state space form

$$\begin{Bmatrix}\dot{Q}\\ \ddot{Q}\end{Bmatrix} = \begin{bmatrix}0 & I\\ -\left[\Omega^2\right] + \left[\overline{A}\right] & 0\end{bmatrix}\begin{Bmatrix}Q\\ \dot{Q}\end{Bmatrix} \tag{13}$$

where $\left[\overline{A}\right] = [\Phi]^T[A][\Phi]$ is the modal aerodynamic influence coefficient matrix. Flutter for this formulation occurs when frequencies coalesce on the imaginary axis and then produce a 90 degree phase shift indicative of increasing amplitude behavior. Divergence occurs when the frequency of oscillation is zero and there is no damping in the system, i.e., when the roots pass through the imaginary axis. These dynamic and static

instabilities can be seen in Figure 4. For the case when the first three modes are used for reduction, the characteristic polynomial is

$$\lambda^6 + p\lambda^4 + q\lambda^2 + r = 0 \tag{14}$$

where the values for the coefficients are

$$p = -(a_{11} - \omega_1^2) - (a_{22} - \omega_2^2) - (a_{33} - \omega_3^2) \tag{15}$$

$$q = (a_{11} - \omega_1^2)(a_{22} - \omega_2^2) + (a_{22} - \omega_2^2)(a_{33} - \omega_3^2) + (a_{33} - \omega_3^2)(a_{11} - \omega_1^2) - a_{12}a_{21} - a_{23}a_{32} - a_{31}a_{13} \tag{16}$$

$$r = -\left|\left[\overline{A}\right] - \left[\Omega^2\right]\right| \tag{17}$$

where $a_{ij}$ denote the coefficients of the modal aerodynamic influence coefficient matrix. Flutter occurs when there is multiplicity of the roots of the characteristic equation.

## System Control Analysis

The addition of forces due to the piezoelectric actuators into the equations of motion is accomplished by adding

$$\{b\} = \begin{Bmatrix} 0 \\ [\Phi]^T\{P\} \end{Bmatrix} \tag{18}$$

where $\{P\}$ is the vector of forces per unit input, into the state space form

$$\{\dot{x}\} = [A]\{x\} + \{b\}u \tag{19}$$

where u is the strain (or voltage) input. For the present problem it is assumed that only one input is used, so u is a scalar and $\{b\}$ is a vector of forces per unit input. Control for this problem is the feedback

$$u = \lfloor g \rfloor\{x\} \tag{20}$$

where $\lfloor g \rfloor$ is the row vector of modal gains, which changes the state space form to the following

$$\begin{Bmatrix} \dot{Q} \\ \ddot{Q} \end{Bmatrix} = \begin{bmatrix} 0 & I \\ \left[\Omega^2\right] + \left[\bar{A}\right] + [\Phi]^T \{P\} \lfloor \mathcal{G} \rfloor & 0 \end{bmatrix} \begin{Bmatrix} Q \\ \dot{Q} \end{Bmatrix} \tag{21}$$

The determination of the gain is dependent on the closed loop poles desired. Pole assignment is the method of specifying the eigenvalue location. Skelton[24] remarks that "eigenvalue location is rarely an adequate statement of control objectives, since the eigenvectors, the zeros, the cost function, and the output correlation are all ignored in this control objective." The understanding of modal behavior with increasing airspeed will allow the implementation of this control concept.

The closed loop characteristic polynomial is desired to be

$$\lambda^6 + \hat{p}\lambda^4 + \hat{q}\lambda^2 + \hat{r} = 0 \tag{22}$$

The gain to assign the poles of the closed loop system to their desired location is

$$\lfloor \mathcal{G} \rfloor = \lfloor \tilde{a} \rfloor^T \left[T_\Delta\right]^{-1} \left[W_\Delta\right]^{-1} \tag{23}$$

with the following definitions

$$\lfloor \tilde{a} \rfloor^T = \lfloor 0 \quad p-\hat{p} \quad 0 \quad q-\hat{q} \quad 0 \quad r-\hat{r} \rfloor \tag{24}$$

$$\left[T_\Delta\right] = \begin{bmatrix} 1 & p & q & & & \\ & 1 & p & q & & \\ & & 1 & p & & \\ & & & 1 & p & \\ & & & & 1 & \\ & & & & & 1 \end{bmatrix} \tag{25}$$

$$\left[W_C\right] = \left[\{b\} \quad [A]\{b\} \quad [A]^2\{b\} \quad \cdots \quad [A]^5\{b\}\right] \tag{26}$$

where the requirement for controllability, $\left|W_C\right| \neq 0$, is for arbitrary $\tilde{a}$.

To change the free vibration frequency of one mode, for example the second mode frequency, $\omega_2$ to $\hat{\omega}_2$, requires the feedback

$$\lfloor \mathcal{G} \rfloor = \left[ 0 \quad \frac{1}{\{U_2\}^T \{P\}} (\omega_2^2 - \hat{\omega}_2^2) \quad 0 \quad 0 \quad 0 \quad 0 \right] \tag{27}$$

The characteristic polynomial of the full equations of motion has been changed by the addition of control coupled terms to the matrix. The changed coefficients of the new characteristic polynomial are

$$\hat{p} = p \tag{28}$$

$$\hat{q} = q - (a_{21} \frac{\{U_1\}^T\{P\}}{\{U_2\}^T\{P\}} + a_{23} \frac{\{U_3\}^T\{P\}}{\{U_2\}^T\{P\}})(\omega_2^2 - \Omega_2^2) \tag{29}$$

$$\begin{aligned} \hat{r} = r + (a_{23}(a_{31} \frac{\{U_1\}^T\{P\}}{\{U_2\}^T\{P\}} - (a_{11} - \omega_1^2) \frac{\{U_3\}^T\{P\}}{\{U_2\}^T\{P\}}) \\ + a_{21}(a_{13} \frac{\{U_3\}^T\{P\}}{\{U_2\}^T\{P\}} - (a_{33} - \omega_3^2) \frac{\{U_1\}^T\{P\}}{\{U_2\}^T\{P\}}))(\omega_2^2 - \Omega_2^2) \end{aligned} \tag{30}$$

The inertially uncoupled system has the terms $\{U_1\}^T\{P\} = \{U_3\}^T\{P\} = 0$; consequently, the change in frequency of the torsion root does not affect the aerodynamic modal behavior of the other modes. The frequencies of all the modes of the coupled system can be changed. Changing the first or third mode will permutate the coefficients in (29) and (30) above. The aerodynamic modal behavior can be modified by changing any one or more modal frequencies in the coupled system.

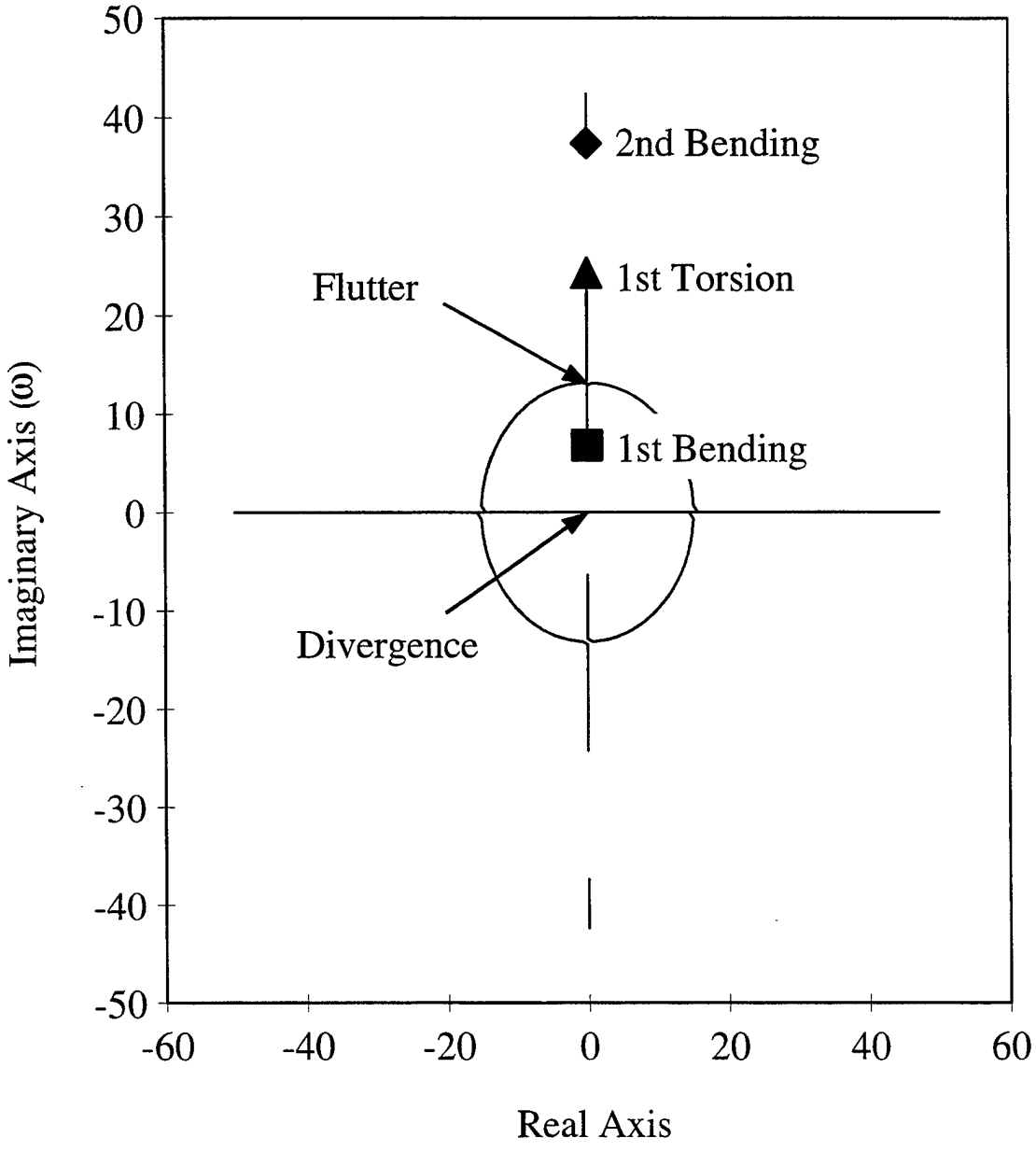


Figure 4. Velocity root locus representation of flutter speed and divergence speed.

# CHAPTER 4

# ILLUSTRATIVE EXAMPLES

To illustrate the present formulations and computational procedures for the flutter analysis and control of wing box type of structures in supersonic flow, a series of illustrative examples have been analyzed with results evaluated numerically and interpreted physically.

## Free Vibration of Wing Box Models

The free vibration natural frequencies and mode shapes were first obtained for a three bay wing box model and compared with those values presented by Striz and Venkayya[17]. The variables used for this comparison were the same as those given in Ref. 18: skin and rib thickness of 0.04 in., web thickness of 0.08 in., and spar cap and vertical post area of 2.0 sq. in. The first six natural frequencies and mode shapes for the three bay wing box model are presented in Figure 5. Good agreement is found as seen in Table 2. The first six natural frequencies and mode shapes for a six bay wing box model were then computed and are presented in Figure 6. As compared to the results for the three bay model, the frequencies and mode shapes for the first three modes are in good agreement, but not in the three other higher modes. The three bay model did not have enough degrees of freedom to accurately model the second torsion, third bending, and third torsion modes. The first six natural frequencies and mode shapes for a six bay wing box with non-structural masses attached to the rear spar are presented in Figure 7. The non-structural masses were attached in order to represent a more realistic wing with stores,

fuel, and control surface actuation mechanisms. These masses were assumed to equal the mass of the original box structure. The natural frequencies are smaller in magnitude than those for the wing box without attached non-structural masses, and the mode shapes exhibit bending and torsion coupling.

To study the trends of free vibration behavior, the thicknesses of the skins, webs, and ribs were varied with the cross sectional areas of the spar caps and vertical posts held at a constant value of 1.0 sq. in. The natural frequencies of the first three modes are presented in Figure 8. The first torsion and second bending frequencies cross at a thickness of 0.126 in. All three frequencies increase rapidly at the thickness values less than, say, 0.01", but both bending mode natural frequencies level off. For the present class of wing boxes, the increase in bending rigidity due to the increase in web and skin thickness is canceled by the increase in masses due to the increase in all three thicknesses. The torsion frequency increases with the thicknesses of the skins, webs and ribs. Obviously, the effect of stiffness increases faster than that of masses.

To further study the trends of free vibration behavior, the cross sectional areas of the spar caps and vertical posts were varied with the thicknesses of the skins, webs, and ribs held at a constant value of 0.1 in. The natural frequencies of the first three modes are presented in Figure 9. The first torsion and second bending frequencies intersect at a cross sectional area of 0.8 sq. in. The increase in spar cap and vertical post cross sectional area has little influence on the first and second bending frequencies. The bending rigidity due to increase in spar cap and vertical post areas is canceled by the increase in masses. The first torsion frequency decreases with increasing areas because the spar caps and vertical posts do not add torsional rigidity, but add mass.

Adding non-structural mass to the rear spar changes the modal behavior of the wing box. The torsion and bending modes have been coupled, especially the first torsion and second bending modes. As an example, it was assumed that the non-structural masses

added equaled the mass of the original box structure. By doing so, the center of mass was always kept at midway between the shear center and the rear spar. With spar cap and vertical post cross sectional areas held at a constant value of 1.0 sq. in., the effect due to the variation of skin, web, and rib thicknesses on natural frequencies of the first three modes are presented in Figure 10. The trends of the first three modes are similar to that in Figure 8 for the lower thickness values, say, below 0.02 inches. From thickness values of 0.04 in. to 0.06 in. the trends are that the second frequency, originally of the first torsional mode, levels off and becomes that of a second bending mode, whereas the third frequency, originally of the second bending mode, keeps increasing and becomes that of a torsional mode. This phenomena of switching of the first torsional and second bending mode is explained by plotting in Figure 11 the migrations of the nodal lines of the two modes as the member thickness increases from 0.02 to 0.1 inches. For member thickness at t=0.02 in., the nodal lines for mode 2 (torsional) and mode 3 (bending) are quite clear. At t=0.04 in., the two lines are migrating. At t=0.06 in., each of the two modes have a mix of torsional and bending modes. At t=0.08 in., mode 2 and mode 3 have switched. At t=0.1 in., the new mode 2 (bending) and mode 3 (torsional) are quite discrete.

The modal behavior of the wing box with attached non-structural masses was further studied by varying the spar cap and vertical post cross sectional areas with the skin, web, and rib thicknesses held at constant value of 0.1 in. The natural frequencies of the first three modes are presented in Figure 12. The trends of the first three modes are similar to that in Figure 9 for the lower thickness values, say, below 1.0 sq. in. For cross sectional areas from 1.5 to 2.5 sq. in., the trends are that the second frequency, originally of the second bending mode, starts decreasing and becomes that of a torsional mode, whereas the third frequency, originally of a first torsion mode, levels off and becomes that of a second bending mode. The switching of the first torsional and second bending modes is illustrated by plotting in Figure 13 the drifting of the nodal line representations of the

two modes as the member cross sectional area increases from 1.0 to 2.6 sq. in. For cross sectional area at a=1.0 sq. in., the nodal lines for mode 2 (bending) and mode 3 (torsion) are distinct. At a=1.4 sq. in., the two lines are migrating. At a=1.8 sq. in., each of the two modes have a mix of torsional and bending modes. At a=2.2 sq. in., mode 2 and mode 3 have switched. At a=2.6 sq. in., the new mode 2 (torsion) and mode 3 (bending) are quite clear.

## Flutter Analyses of Wing Box Models

The flutter predictions were checked for subsonic flow on the three and six bay wing boxes. The variables used were the same as those used to check the free vibration frequencies. The unswept three bay wing box was reported by Striz and Venkayya[17] to have a flutter velocity of 866 feet per second at an altitude of 10,000 feet and a flight Mach number of 0.5566. The aerodynamic theory used for this prediction was the doublet lattice method. Hemmig, Venkayya, and Eastep[25] compare the aerodynamics approximated by the doublet lattice method to that by the linear strip theory and report that the "difference between the flutter speeds computed by these two procedures is approximately 20%, and strip theory is conservative in that it predicts a lower speed." In this study, the frequency coalescence method with linear strip theory yielded the flutter speed to be 686 feet per second, which is approximately 20% on the conservative side. Under the same flight conditions, the divergence speed of a wing swept forward $30^{o}$ with six bays was reported to be 515 feet per second by Bowman, Grandhi, and Eastep[20]. Whereas in this study the divergence speed of such a wing was found to be 525 feet per second. The change in flutter and divergence speeds with sweep in the subsonic regime matched the general trends reported by Bisplinghoff[26].

Supersonic aerodynamics were modeled using a first order high Mach number approximation to the linear potential flow theory with damping terms neglected, the

aerodynamic center located at the half chord. The conditions were assumed to be flight at Mach 2.0, at an altitude of 20,000 ft., with the wing swept back at an angle of $30^{o}$ with respect to the free stream.

Supersonic flutter by the method of frequency coalescence using strip theory aerodynamics is examined for the six bay wing boxes with the same variables used to check the free vibration frequencies. Flutter for the wing box without attached non-structural masses is shown in Figure 14 to involve the coalescence of the first torsion and second bending frequencies. The first torsion frequency increases due to increasing airspeed because the nodal line is in front of the line of aerodynamic centers in the supersonic regime. Flutter for the wing box with non-structural masses attached to the rear spar is shown in Figure 15 to involve the coalescence of the first and second modes. The second mode frequency decreases due to increasing airspeed because it is a torsion-type mode with the nodal line aft of the line of the aerodynamic centers in the supersonic regime. It should be mentioned that there is a marked decrease in the flutter speed for the wing box with attached non-structural masses.

To study the trends of flutter behavior, the thicknesses of the skins, webs, and ribs were varied for several cross sectional areas of the spar caps and vertical posts. The flutter velocities for the spar cap and vertical post cross sectional areas ranging from 0.5 to 1.5 sq. in. are presented in Figure 16. The mode of flutter involves the first torsion and second bending frequencies. The thickness value at which the frequencies of these two modes cross is worthy of special mention. At this crossing point, the frequency for the first torsional mode and that of the second bending mode are the same at zero free stream velocity, or zero flutter speed. The flutter velocity is zero at a skin, web, and rib thickness of 0.126 in. for the spar cap and vertical post cross sectional area of 1.0 sq. in. This crossing point corresponds to that reported earlier for the free vibration analysis. Increasing the spar cap and vertical post cross sectional areas moves this crossing point to

higher skin, web, and rib thicknesses, whereas decreasing the member areas moves this crossing point to lower member thickness values.

To further study the trends of flutter behavior, the cross sectional areas of the spar caps and vertical posts were varied for several thicknesses of the skins, webs, and ribs. The flutter velocities for the skin, web, and rib thicknesses ranging from 0.05 to 0.15 in. are presented in Figure 17. The frequency crossing point which corresponds to zero flutter speed is seen to occur at a cross sectional area of 0.8 sq. in. for the skin, web, and rib thickness of 0.10 in. Increasing the skin, web, and rib thickness moves this crossing point to higher spar cap and vertical post cross sectional areas, whereas decreasing the member thicknesses moves this crossing point to lower member thickness values.

The flutter behavior of the wing box is changed with the addition of non-structural mass to the rear spar. The non-structural masses added are assumed to be equal to the mass of the original box structure, which is consistent with the free vibration analysis. The effect due to the variation of skin, web, and rib thickness for spar cap and vertical post cross sectional areas ranging from 0.5 to 1.5 sq. in. are presented in Figure 18. For example, there is a significant drop in flutter speed at a skin, web, and rib thickness of 0.054 in. for the spar cap and vertical post cross sectional area of 1.0 sq. in. This drop in flutter velocity is due to the switching from mode 1 and mode 2 coalescence (left hand side of the curve) to mode 2 and mode 3 coalescence (right hand side of the curve). As demonstrated in Figure 18, adding the non-structural masses to the rear spars, which is a more realistic model, has an effect of eliminating those zero value cusps of the flutter curves as shown in Figure 16, moving the flutter curves to higher values with the bottom envelope values ranging from 600 to 900 feet per second. Increasing the spar cap and vertical post cross sectional areas moves this switching point to higher skin, web, and rib thicknesses, whereas decreasing the member areas moves this switching point to lower member thickness values.

The flutter behavior of the wing box with attached non-structural masses was further studied by varying the spar cap and vertical post cross sectional areas. The effect due to the variation of spar cap and vertical post cross sectional areas for skin, web, and rib thickness ranging from 0.5 to 1.5 sq. in. are presented in Figure 19. For example, there is a significant increase in flutter velocity at a spar cap and vertical post cross sectional area of 1.9 sq. in. for the skin, web, and rib thickness of 0.1 in. This jump in flutter velocity is due to the switching from mode 2 and mode 3 coalescence (left hand side of the curve) to mode 1 and mode 2 coalescence (right hand side of the curve). As in the case of varying the thicknesses of the skins, webs, and ribs, the zero value cusps of the flutter curves, as seen in Figure 17, have been eliminated and the bottom envelope ranges from 700 to 1400 feet per second. Increasing the skin, web, and rib thicknesses moves this switching point to higher spar cap and vertical post cross sectional areas, whereas decreasing the member thicknesses moves this switching point to lower member thickness values.

## Flutter Control of Wing Box Models

The control of the wing box was implemented by adding piezoelectric elements and feeding back the modal gain which produces the desired free vibration frequency. The piezoelectric actuators were assumed to have twice the thickness of the skins, webs, and ribs. When the piezoelectrical strips were added as shown in Figure 3, it was assumed that the resulted additional stiffnesses and masses were too small to affect the frequencies as compared to the effect due to the stresses induced by the strips.

To study the trends of controlling flutter, the skin, web, and rib thicknesses were varied for several controlled values of the torsional frequency. The spar cap and vertical post cross sectional areas were held at a constant value of 1.0 sq. in. The flutter velocities for the modified torsional frequencies ranging from -10% to +10% of the uncontrolled

frequency are presented in Figure 20. The similarities between these results due to frequency control and those due to changes in spar cap and vertical post cross sectional areas as shown in Figure 16 are evident. It is noted that for 0% torsional frequency change, the pattern of the curve is identical to that as shown in Figure 16 with spar cap and post cross sectional area of 1.0 sq. in. Lowering the torsional frequency is equivalent to increasing the spar cap and vertical post area which moves the crossing point to a higher skin, web, and rib thickness. Raising the torsional frequency is equivalent to lowering the member areas which moves the crossing point to higher member thickness values.

Control of the wing box with non-structural masses distributed on the rear spar is complicated due to the control and aerodynamic coupled terms in Eqs. (29) and (30). To be consistent with the previous analyses, the non-structural masses were again assumed to be equal to the mass of the original box structure. Because of the modal coupling, any one or more of the frequencies can be changed with appropriate feedback. The effect due to the variation of skin, web, and rib thickness, with spar cap and vertical post cross sectional areas held at a constant value of 1.0 sq. in., for the modified mode 3 frequency ranging from -10% to +10% are presented in Figure 21. It is noted that for 0% mode 3 frequency change, the pattern of the curve is identical to that as shown in Figure 18 with spar cap and post cross sectional area of 1.0 sq. in. Changing the mode 3 frequencies result in flutter curves of the same patterns as those shown in Figure 18.

## Weight Comparisons for Controlled Wing Boxes

The requirement for minimum flutter speeds and the requirement for structural strength due to static equivalent lift load must be met by any design choice of skin, web, and rib thicknesses, and the spar cap and vertical post areas. An alternative approach is to select these variables to meet the strength requirement and to implement control

devices to meet the flutter requirement. The weight of the design could become the deciding factor when weighing the pros and cons of the two choices. The spar caps are assumed to primarily carry the bending stress of the static equivalent lift load. The spar cap area which is of sufficient size to meet margin of safety requirements was assumed to be 1.0 sq. in. in this example. The flutter requirement for flight at Mach 2.0 and an altitude of 20,000 ft. was assumed to be 2500 feet per second for this example.

For the wing box without distributed non-structural masses, the flutter requirements can be met for a skin, web, and rib thickness of 0.15 in. as shown in Figure 20. The wing box with piezoelectric actuators increasing the torsional frequency by 10% would meet the same flutter requirements at a skin, web, and rib thickness of 0.09 in. as shown in Figure 20. The wing box with piezoelectric actuators weighs 243 lbs. whereas the weight of the wing box with the thicker skins, webs, and ribs is 222 lbs.

For the wing box with distributed non-structural masses, the flutter requirements can be met for a skin, web, and rib thickness of 0.23 in. as shown in Figure 21. The piezoelectric actuators increasing the third mode frequency by 10% would meet the flutter requirement at a thickness of 0.17 in. as shown in Figure 21. The weight of the wing box with piezoelectric actuators is 353 lbs. whereas the weight of the wing box with thicker skins, webs, and ribs is 331 lbs. There is a weight penalty associated with the actuators due to the fact that the decrease in skin, web, and rib thickness is small compared to the relative size of the piezoelectric actuators necessary to implement the frequency changes.

For all cases, the trends show that for larger spar cap and vertical post areas, there is the possibility of meeting the flutter requirements at lower skin, web, and rib thicknesses. To elaborate the advantage of using piezoelectric actuators for weight saving on the wing box without attached non-structural masses, Figure 22 is shown. It is seen that for the skin, web, and rib thickness of 0.06 in., the flutter speed limitation of 2500 feet per second can be met by sufficiently decreasing the torsional frequency of the wing

box by 54%, or increasing the torsional frequency of the wing box by 21%. Without piezoelectric actuators, to achieve this flutter requirement a spar cap and vertical post cross sectional area of 2.15 square inches is needed. The weight of the wing box with piezoelectric actuators is 174 lbs. whereas the weight of the wing box with larger spar caps and vertical posts is 231 lbs.

The wing box with attached non-structural masses can meet the flutter requirement of 2500 feet per second at a skin, web, and rib thickness of 0.11 in. by using the piezoelectric actuators to increase the third mode frequency by 36%, as shown in Figure 23. This requirement can also be met by a wing box with a spar cap and vertical post cross sectional area of 2.15 square inches. The weight of the wing box with piezoelectric actuators is 255 lbs. whereas the weight of the wing box with larger spar caps and vertical posts is 286 lbs.

Table 2. Comparison of natural frequencies of the three bay wing box model.

| Mode Shape | Three Bay Wing Box (Present Study) | Three Bay Wing Box (Ref. 17) | Percentage Difference |
|---|---|---|---|
| 1st Bending | 6.30 | 6.26 | 0.6 |
| 1st Torsion | 24.77 | 24.75 | 0.1 |
| 2nd Bending | 37.06 | 37.57 | 1.4 |
| 2nd Torsion | 71.90 | 71.77 | 0.2 |
| 3rd Bending | 110.98 | 110.35 | 0.6 |
| 3rd Torsion | 123.79 | 122.65 | 0.9 |

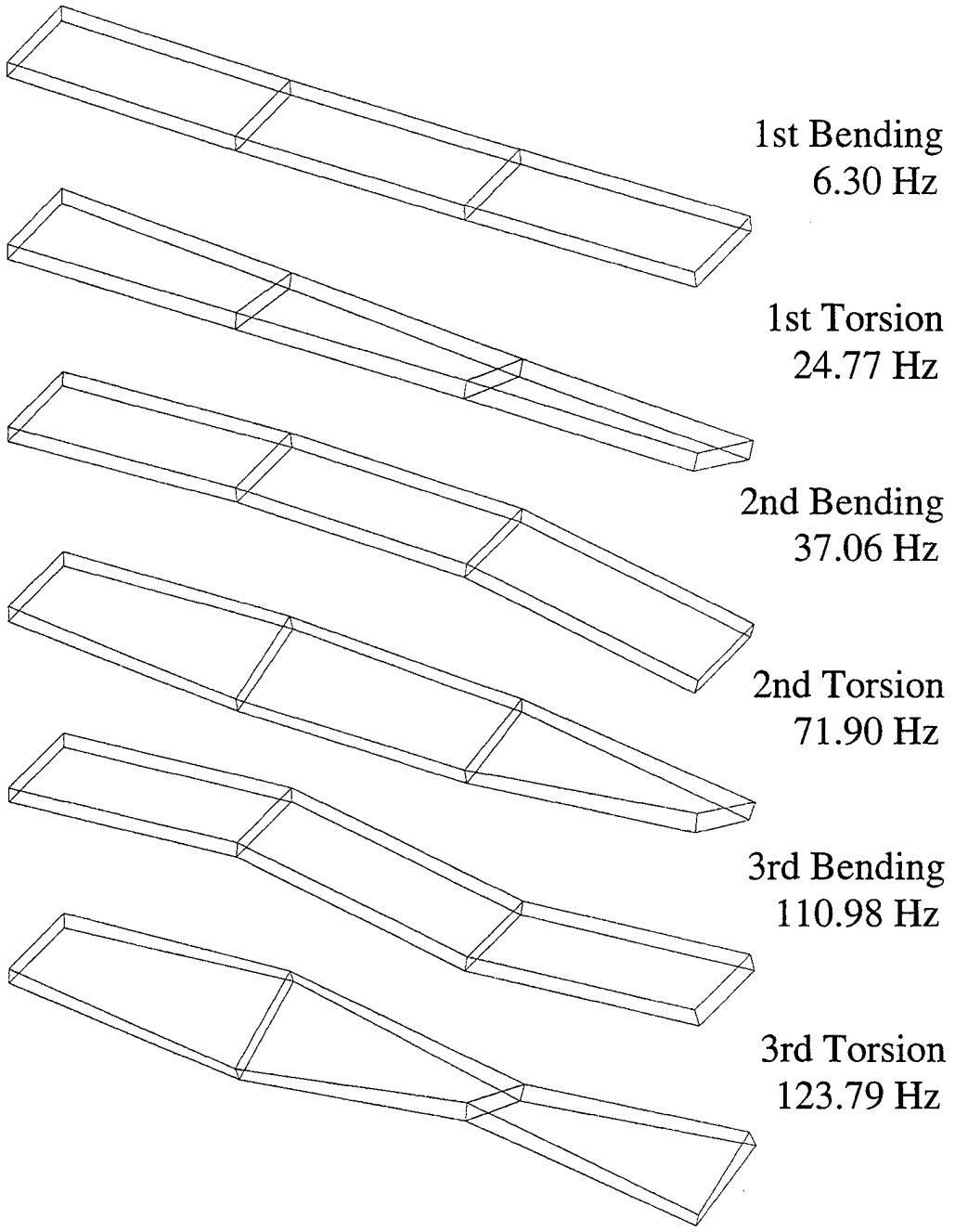


Figure 5. Natural frequencies and mode shapes for the first six modes of the three bay wing box without non-structural masses.

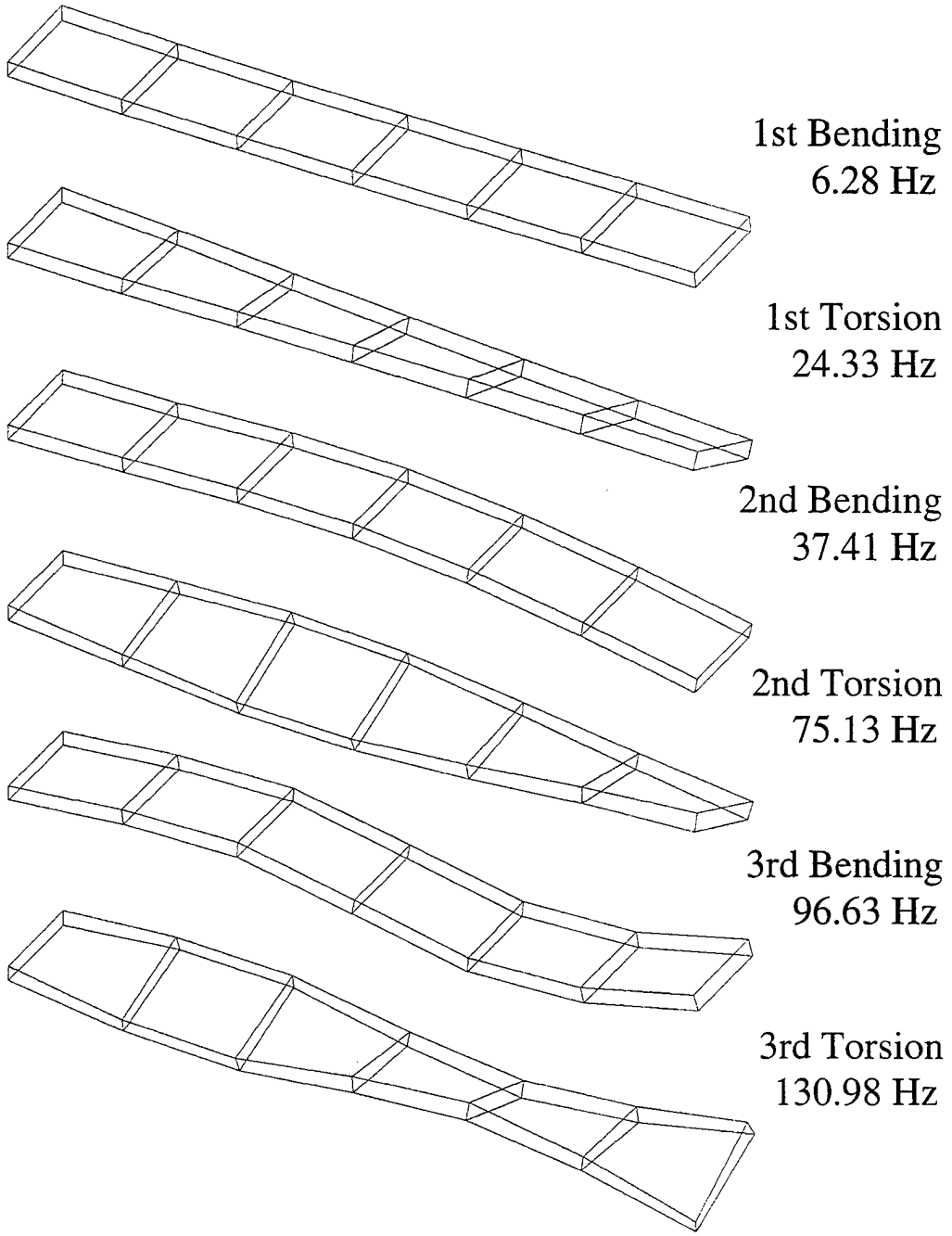


Figure 6. Natural frequencies and mode shapes for the first six modes of the six bay wing box without non-structural masses.

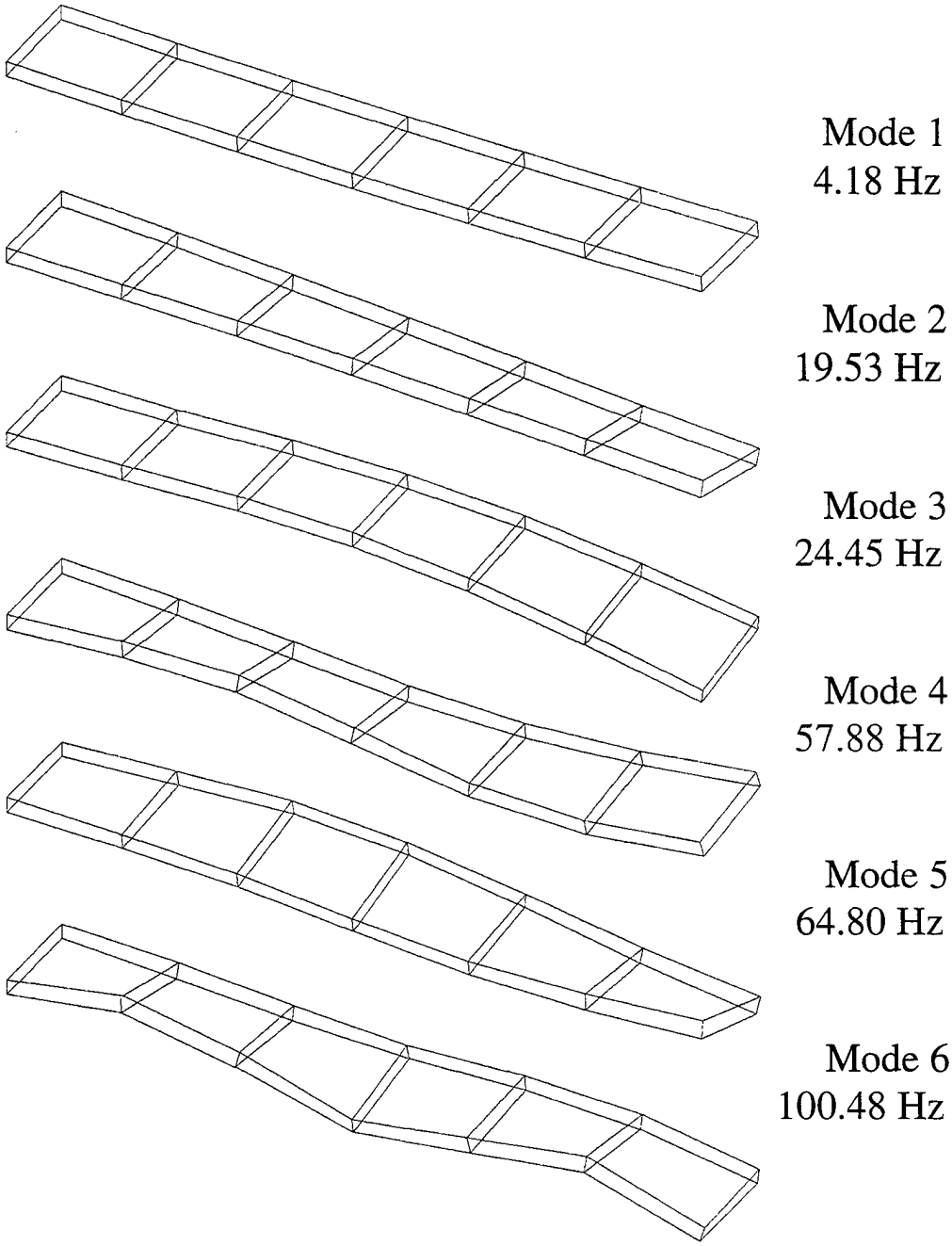


Figure 7. Natural frequencies and mode shapes for the first six modes of the six bay wing box with non-structural masses.

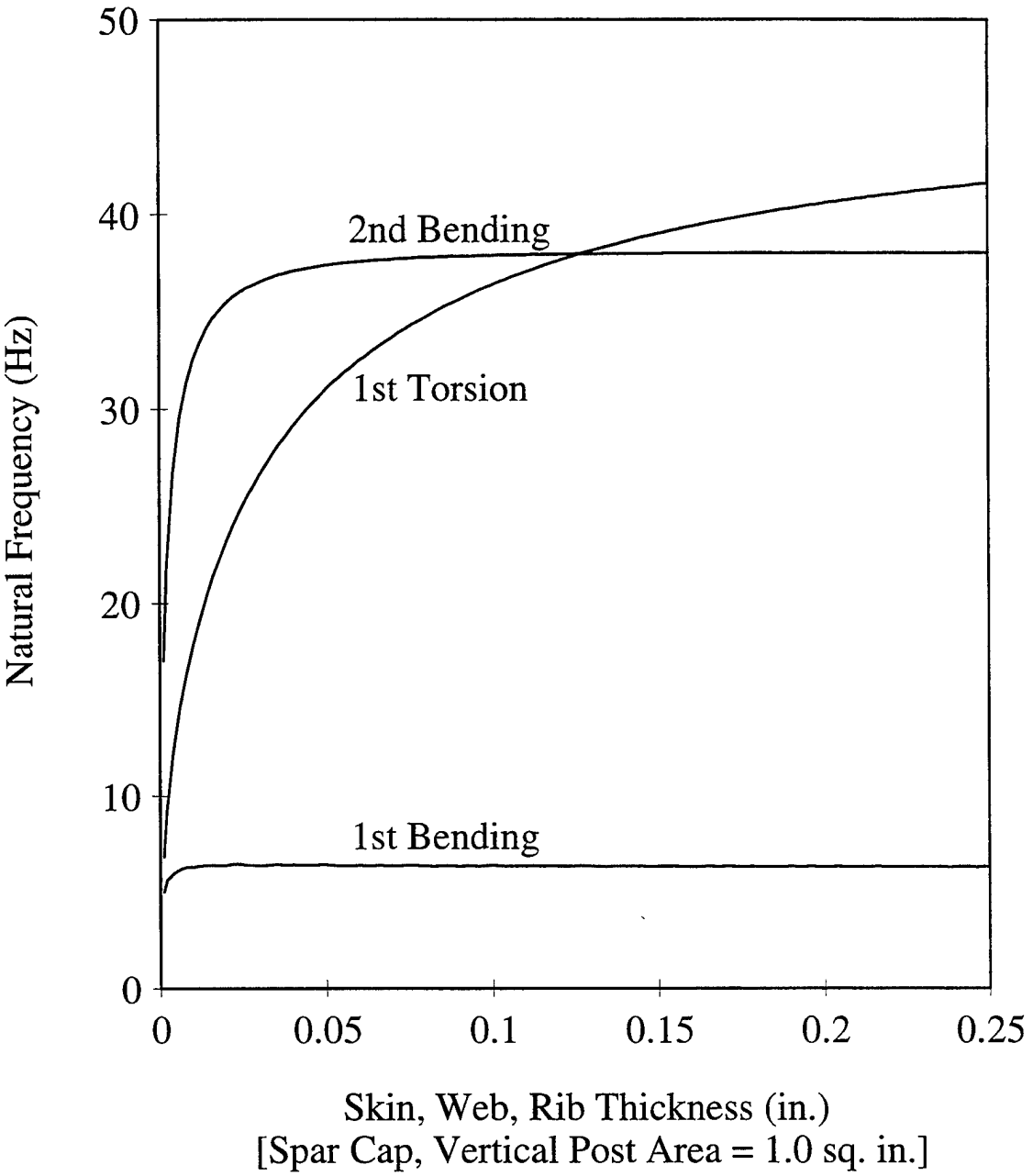


Figure 8. Effect of skin, web, and rib thickness on the first three natural frequencies of the wing box without non-structural masses.

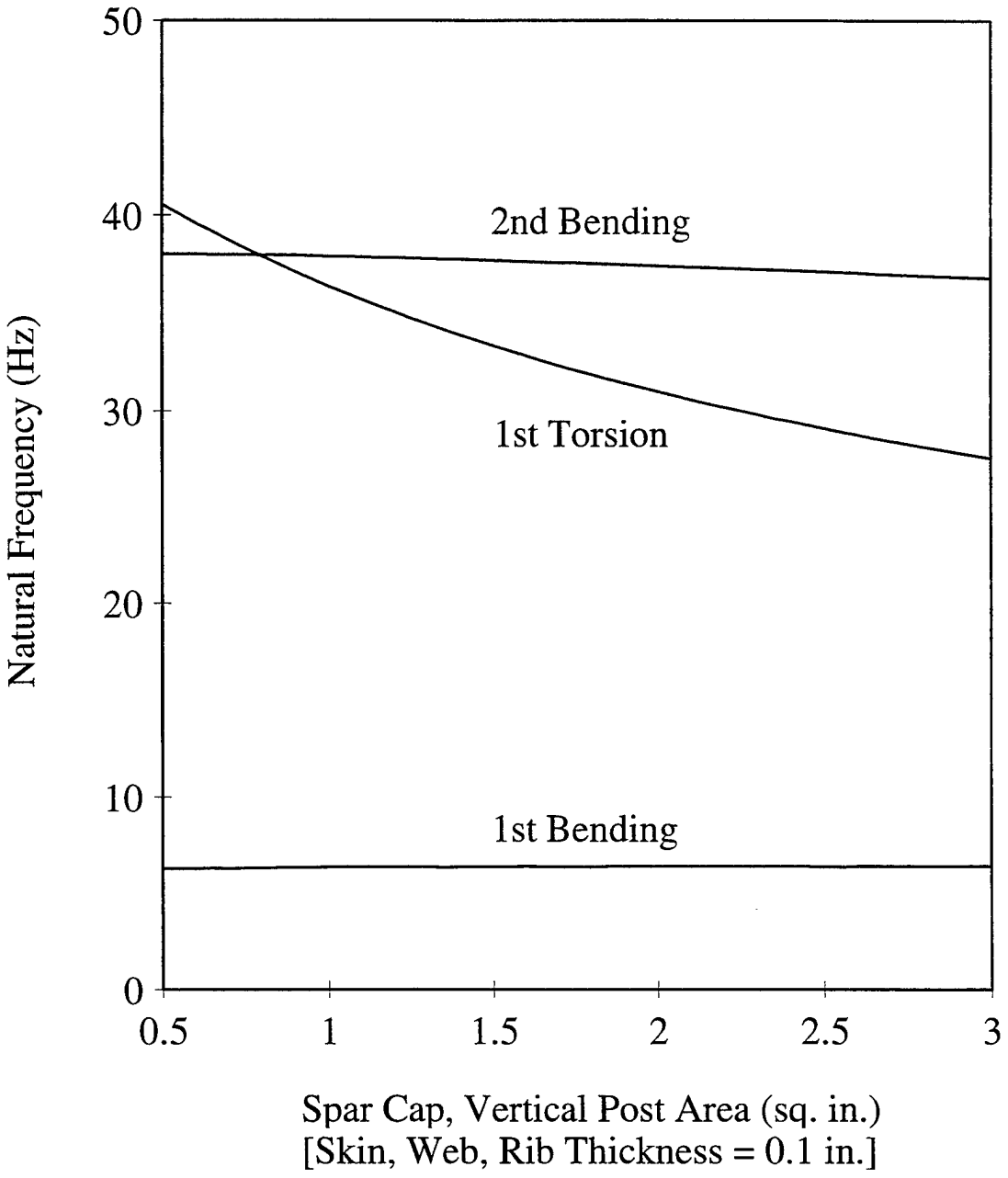


Figure 9. Effect of spar cap and vertical post cross sectional area on the first three natural frequencies of the wing box without non-structural masses.

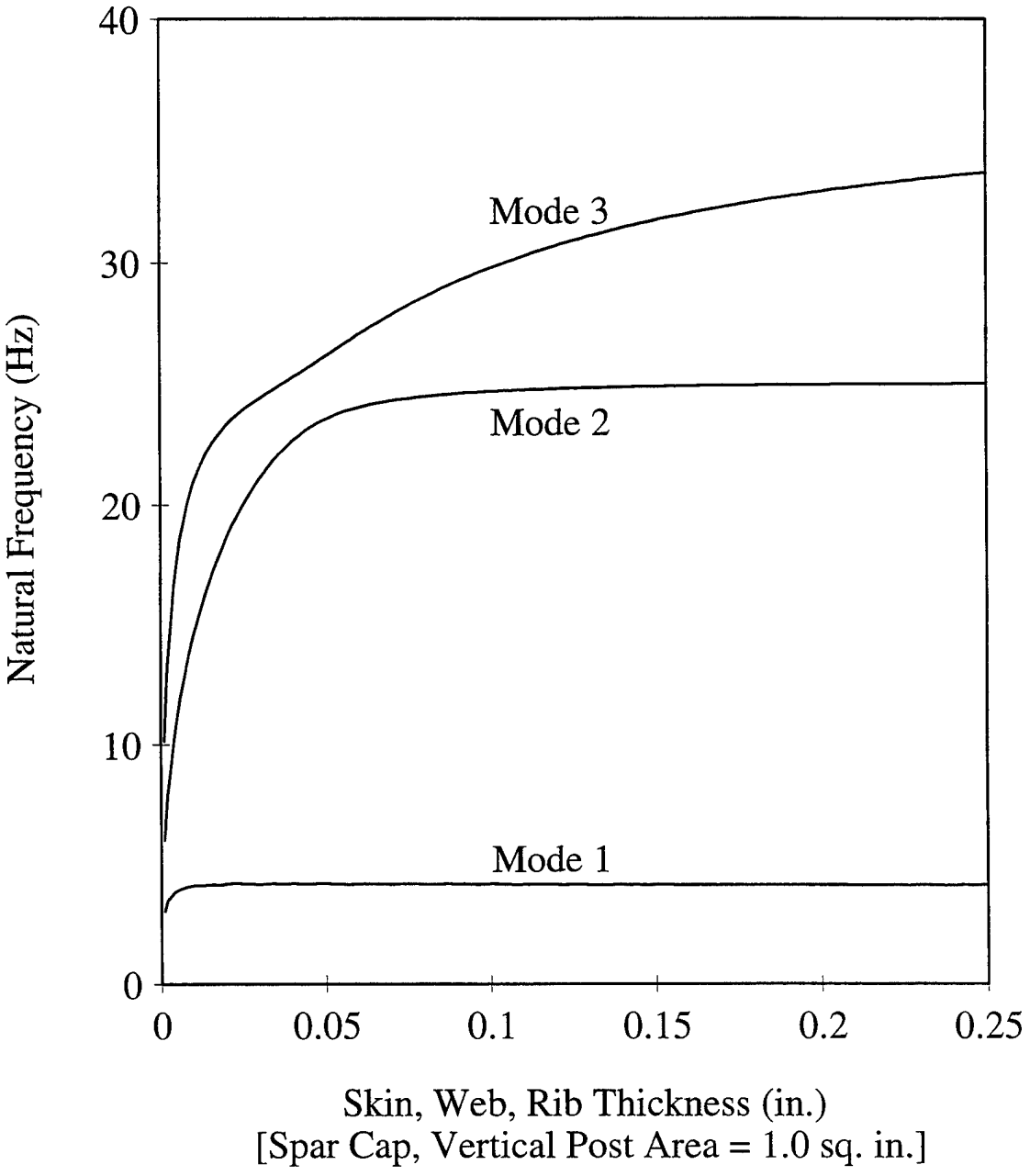


Figure 10. Effect of skin, web, and rib thickness on the first three natural frequencies of the wing box with non-structural masses.

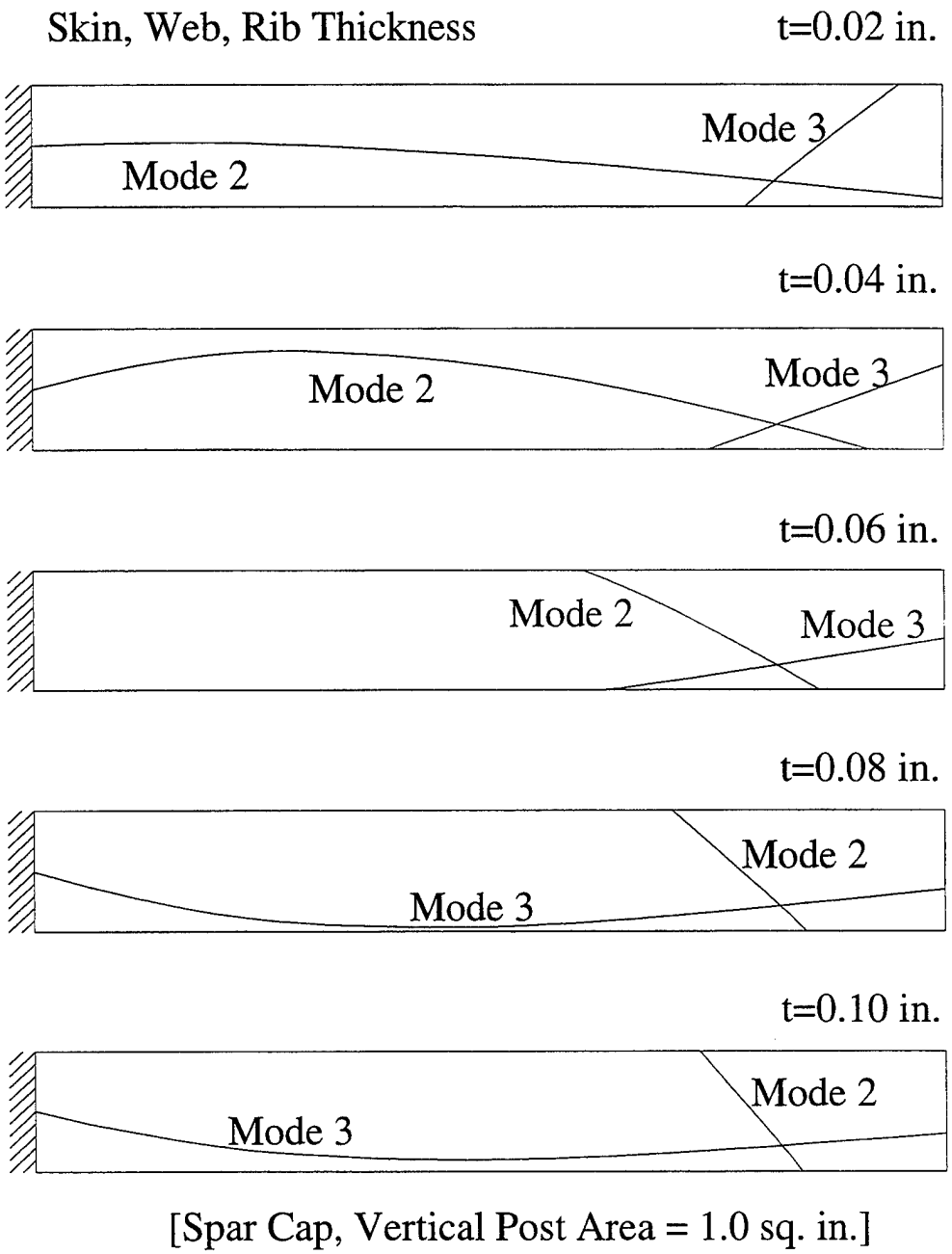


Figure 11. Effect of skin, web, and rib thickness on the nodal line representations for the second and third mode shapes of the wing box with non-structural masses.

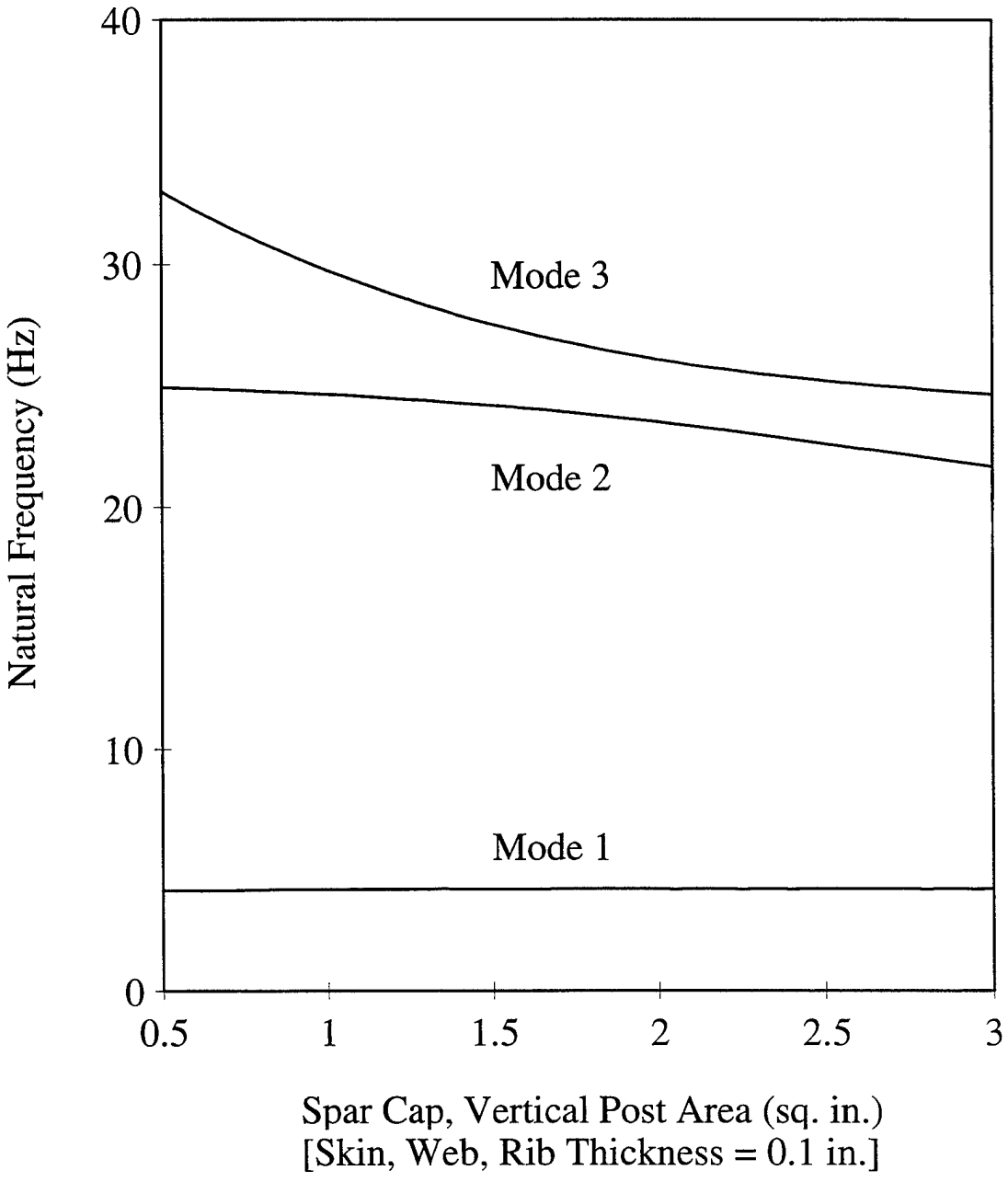


Figure 12. Effect of spar cap and vertical post cross sectional area on the first three natural frequencies of the wing box with non-structural masses.

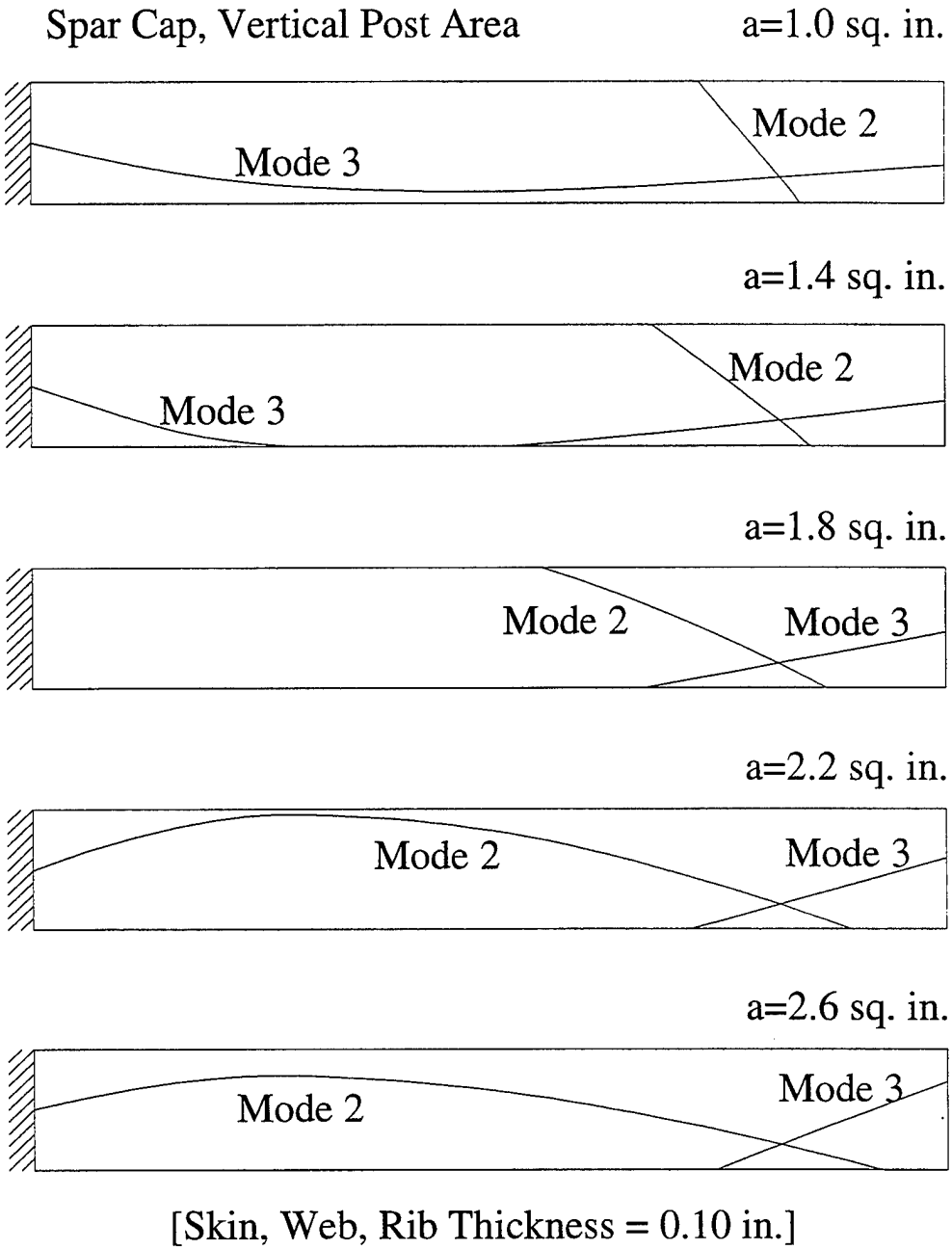


Figure 13. Effect of spar cap and vertical post cross sectional area on the nodal line representations for the second and third mode shapes of the wing box with non-structural masses.

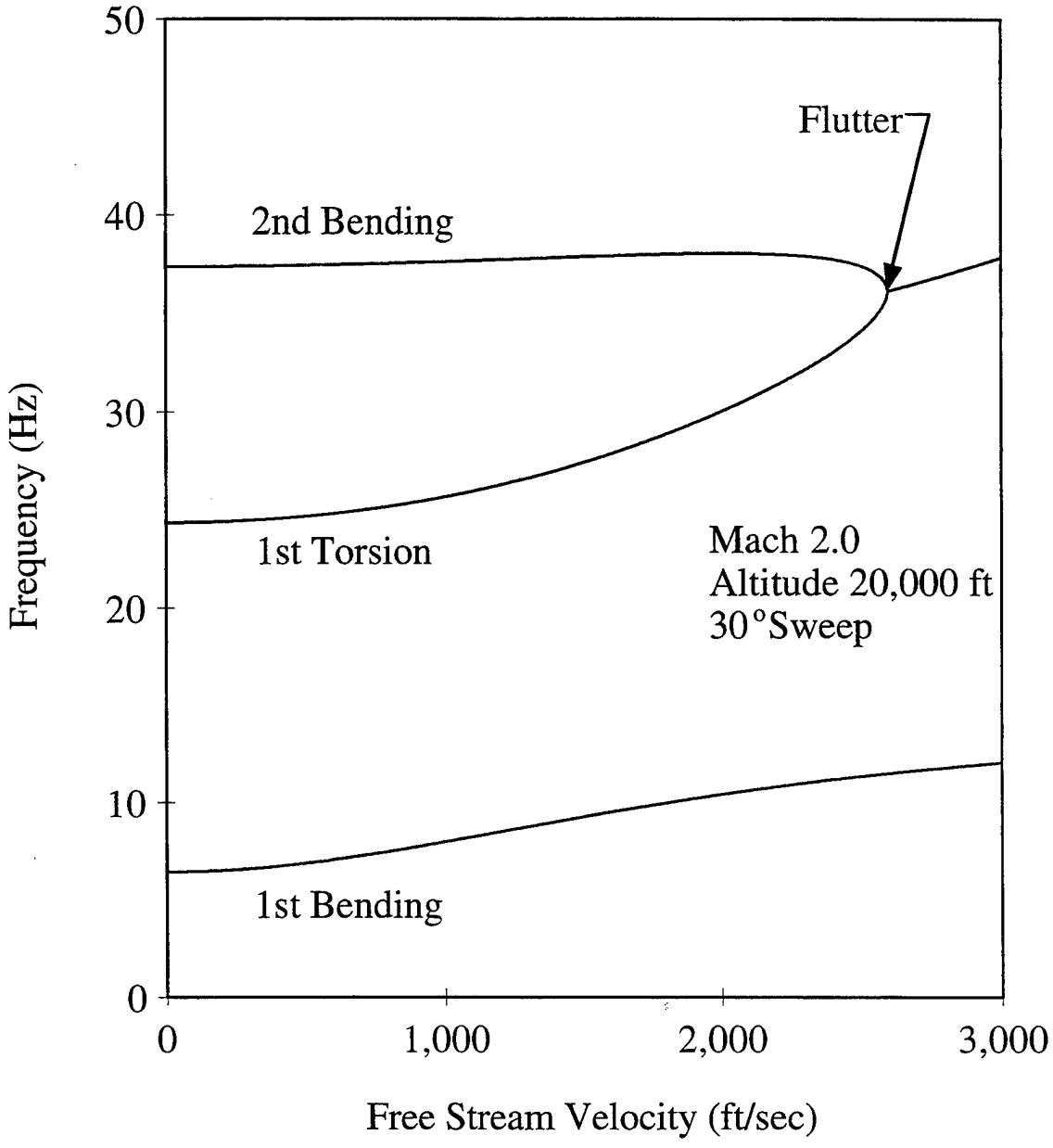


Figure 14. Frequency coalescence of the first three natural frequencies of the wing box without non-structural masses.

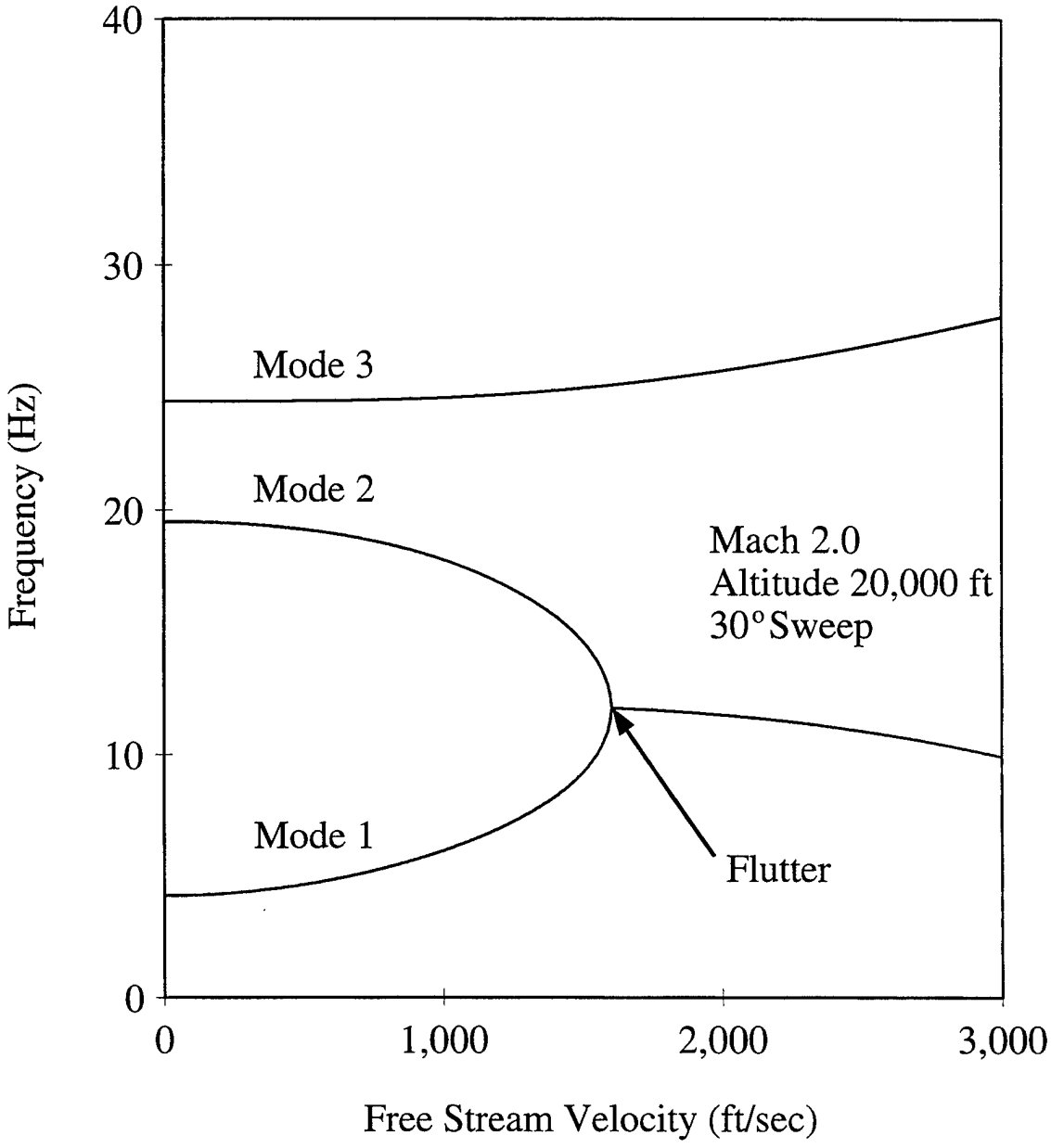


Figure 15. Frequency coalescence of the first three natural frequencies of the wing box with non-structural masses.

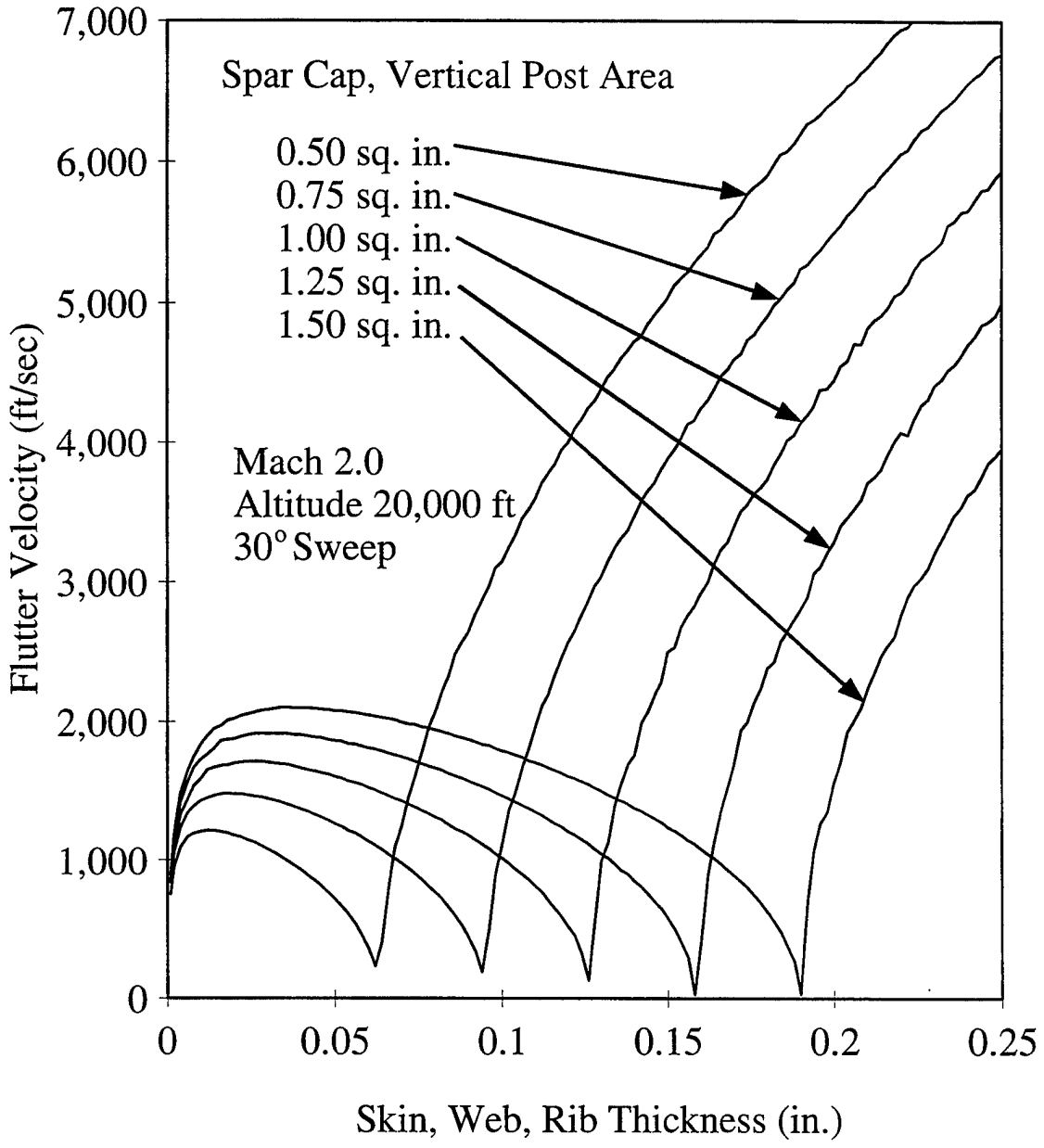


Figure 16. Effect of skin, web, and rib thickness on the flutter speed for specified spar cap and vertical post cross sectional areas of the wing box without non-structural masses.

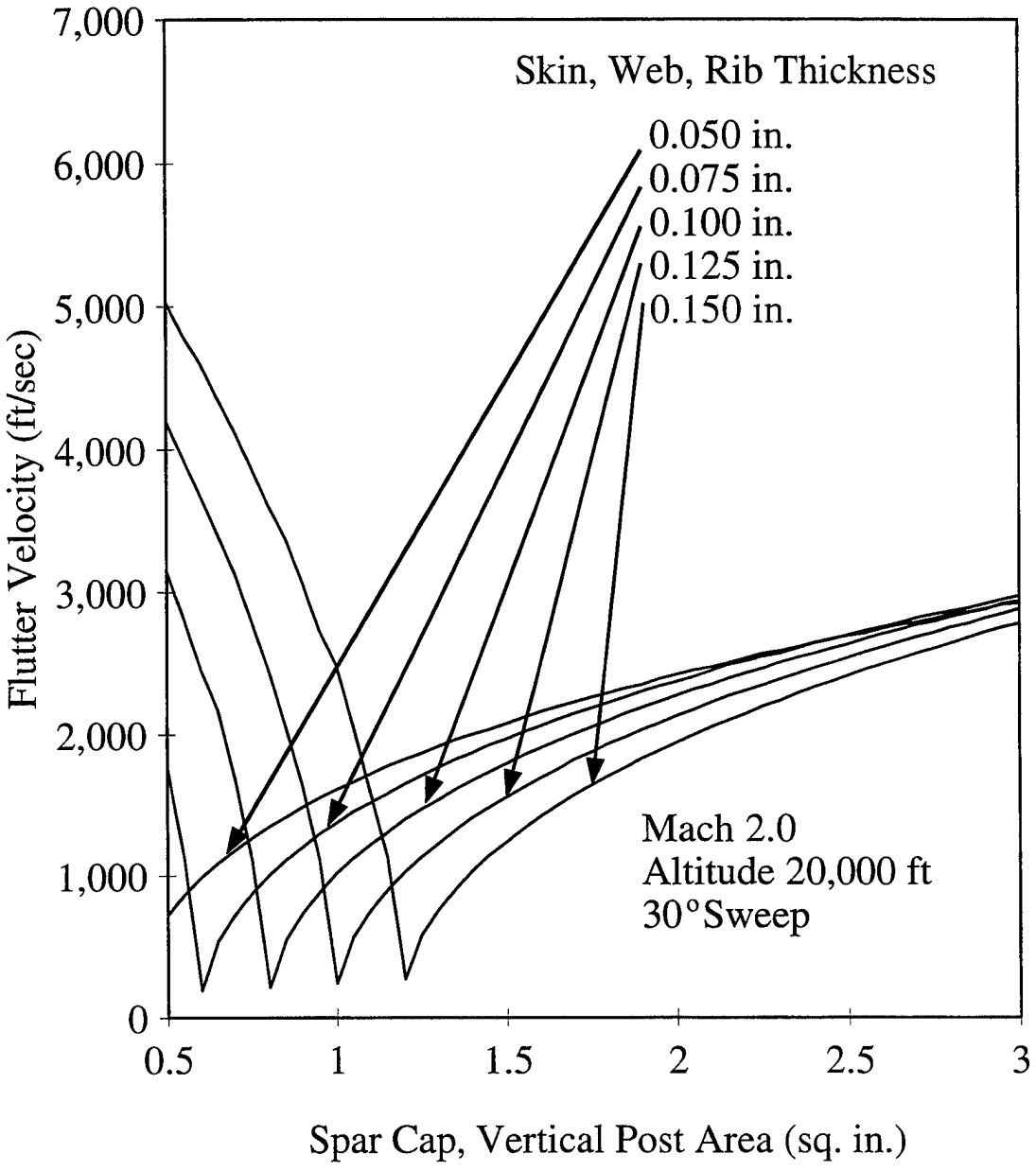


Figure 17. Effect of spar cap and vertical post cross sectional area on the flutter speed for specified skin, web, and rib thicknesses of the wing box without non-structural masses.

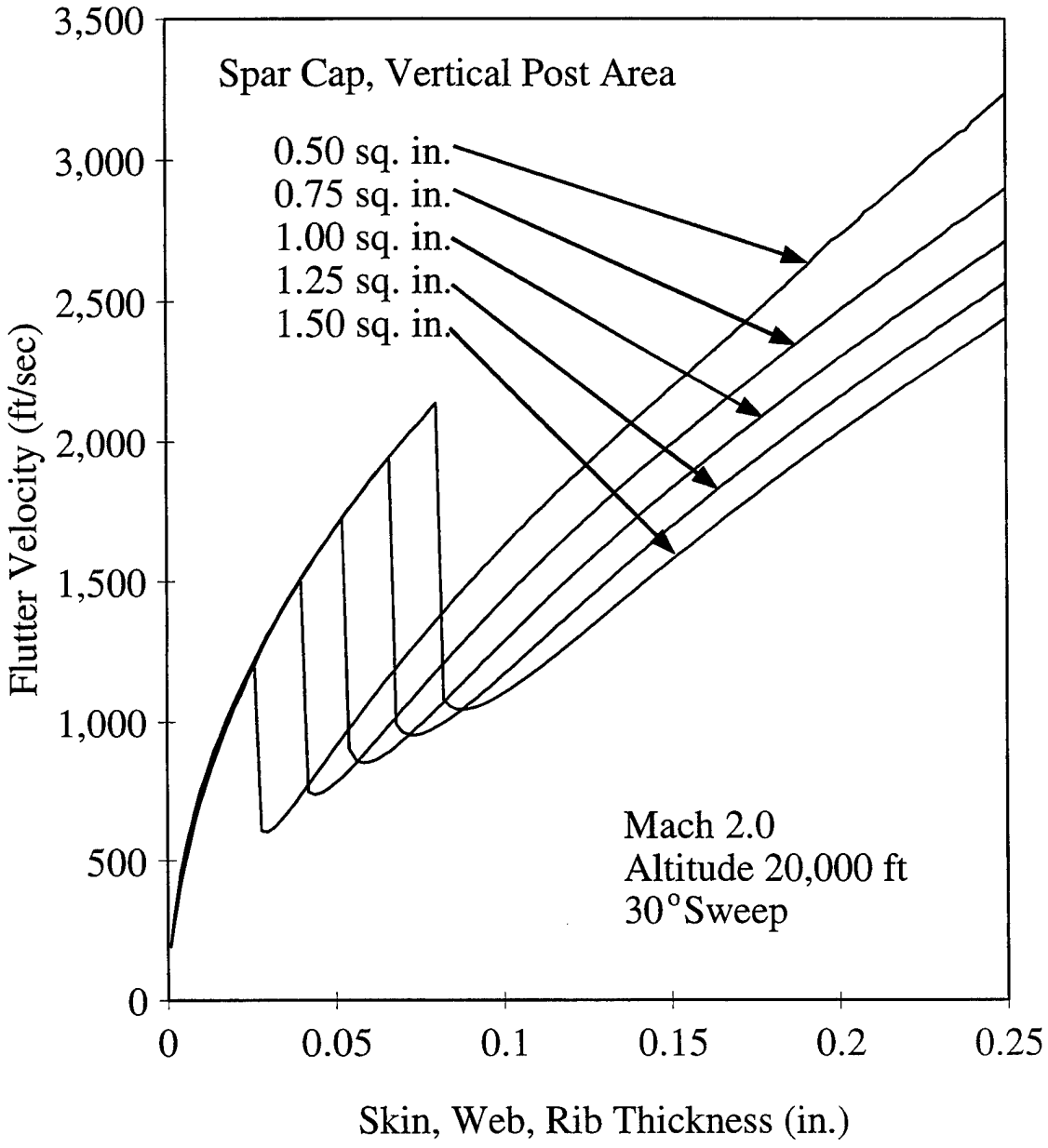


Figure 18. Effect of skin, web, and rib thickness on the flutter speed for specified spar cap and vertical post cross sectional areas of the wing box with non-structural masses.

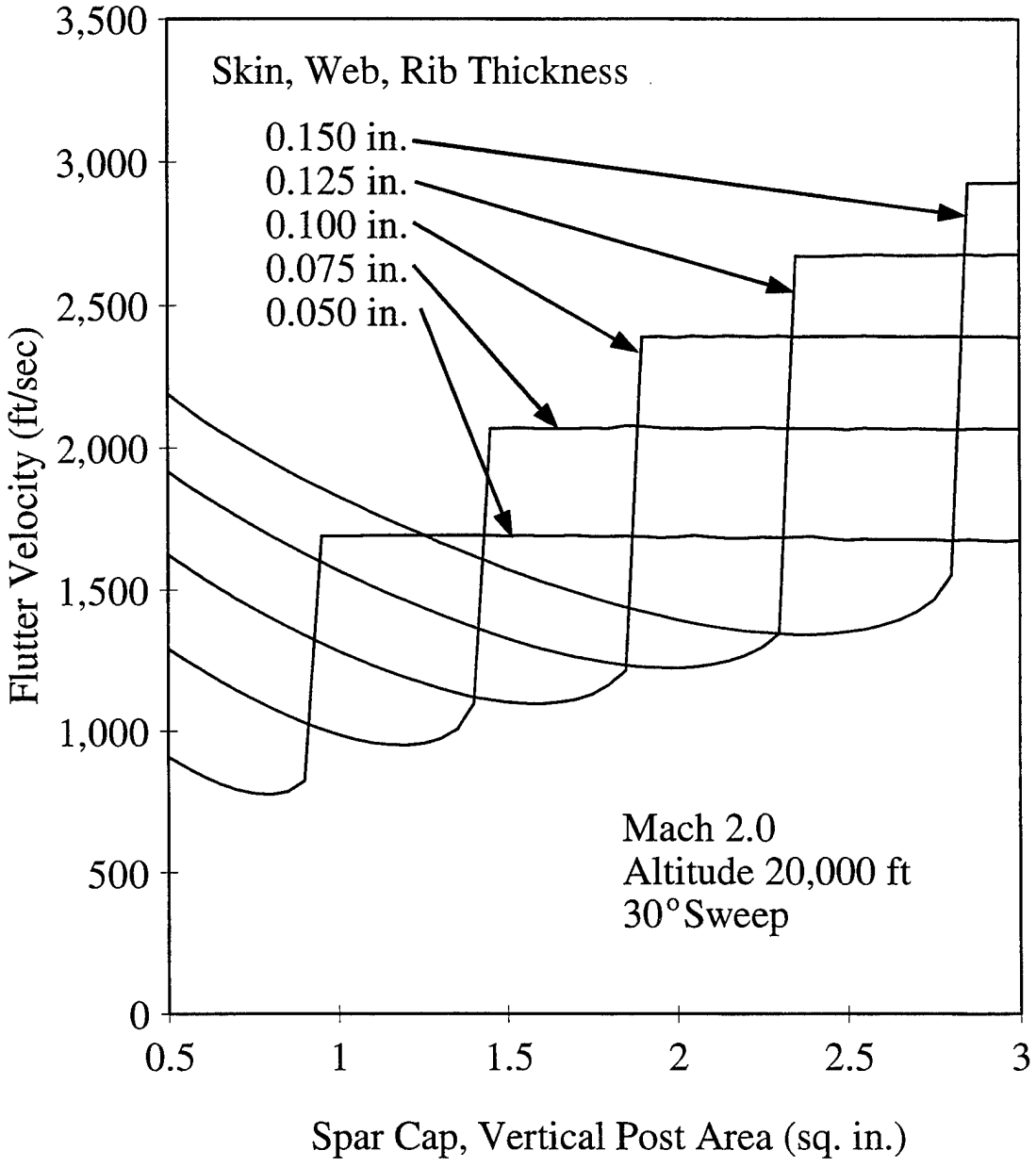


Figure 19. Effect of spar cap and vertical post cross sectional area on the flutter speed for specified skin, web, and rib thicknesses of the wing box with non-structural masses.

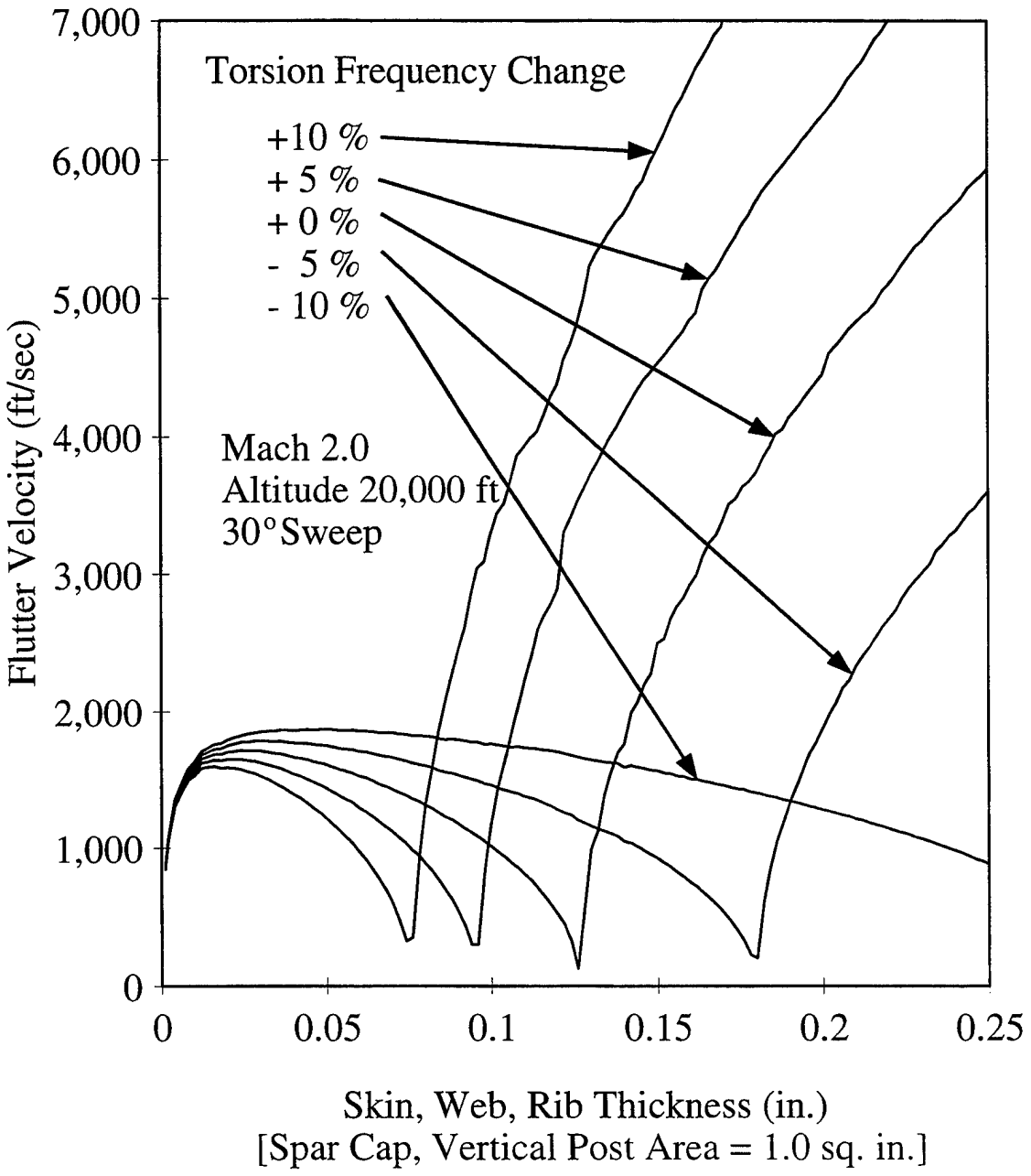


Figure 20. Effect of skin, web, and rib thickness on the flutter speed with torsion frequency change of the wing box without non-structural masses.

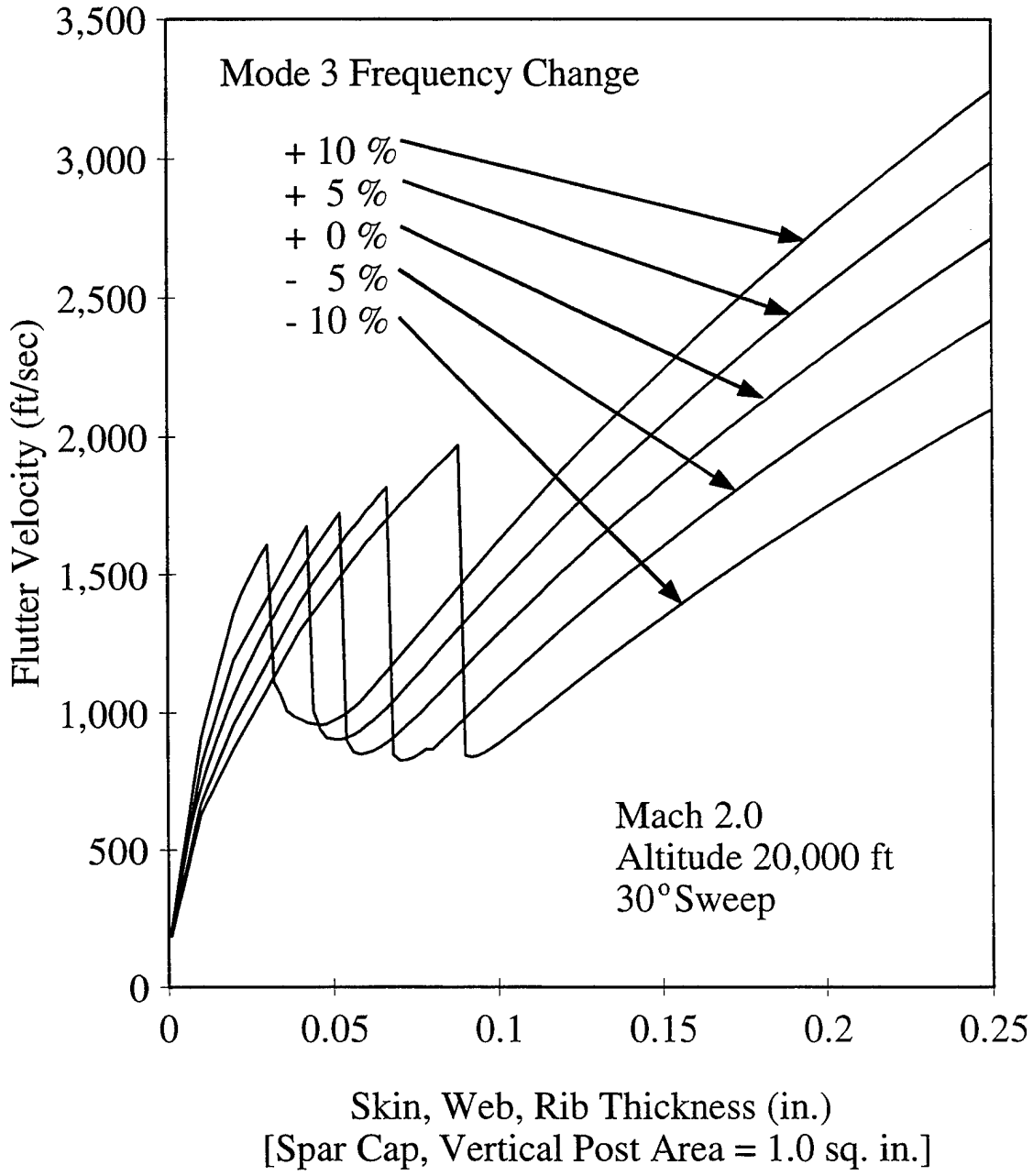


Figure 21. Effect of skin, web, and rib thickness on the flutter speed with third mode frequency change of the wing box with non-structural masses.

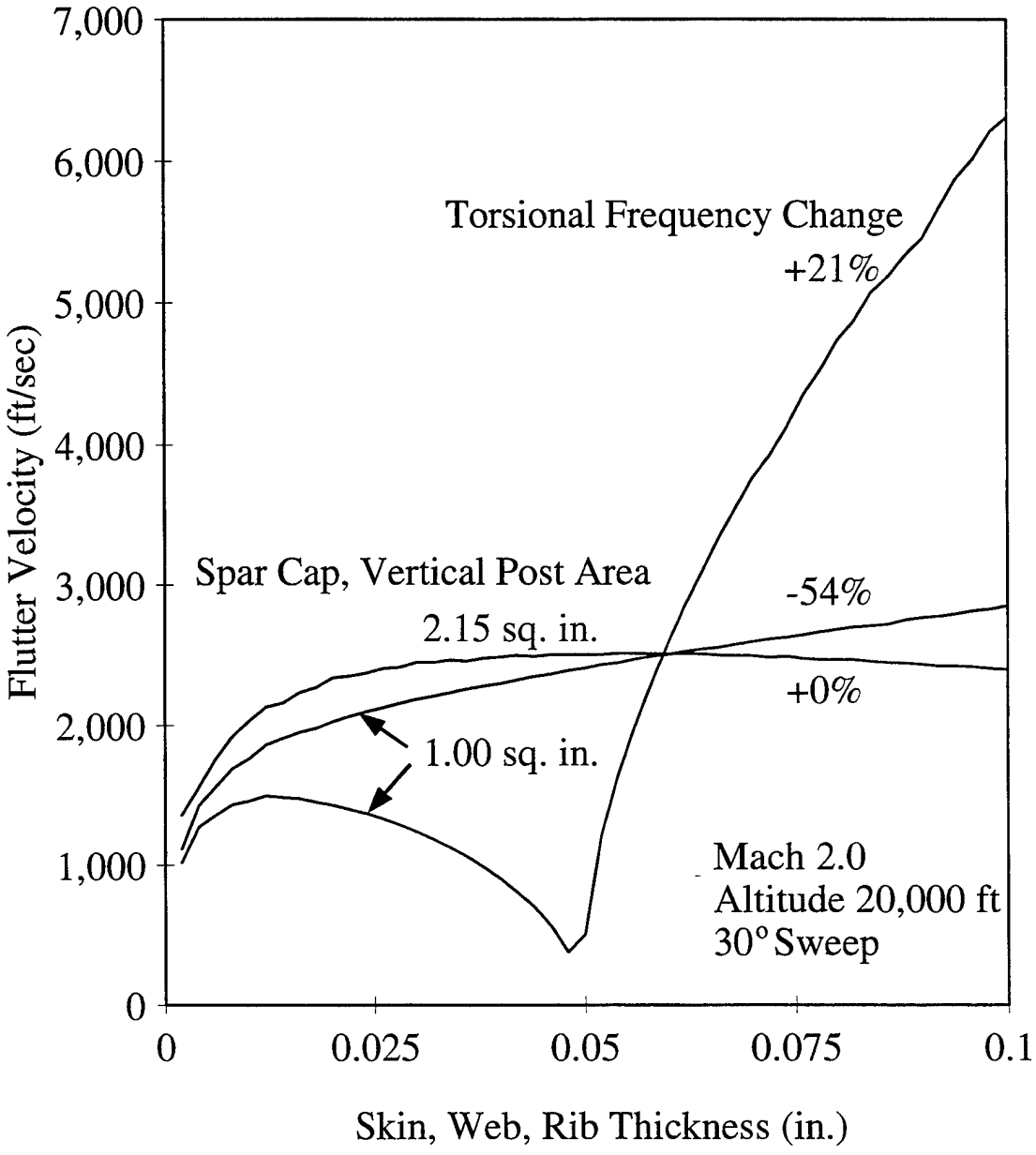


Figure 22. Effect of spar cap and vertical post cross sectional area and torsion frequency change to meet the flutter requirement of the wing box without non-structural masses.

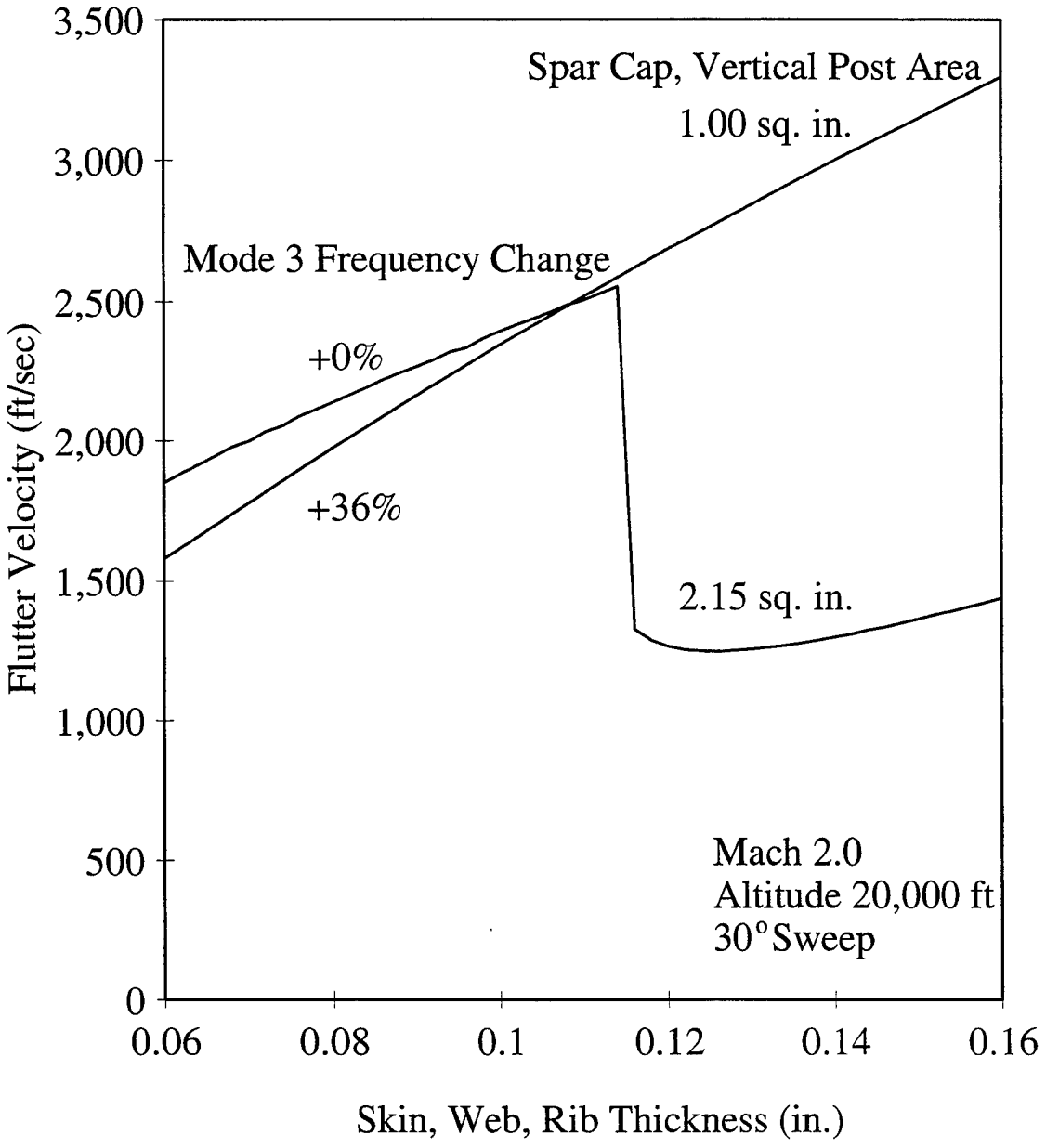


Figure 23. Effect of spar cap and vertical post cross sectional area and third mode frequency change to meet the flutter requirement of the wing box with non-structural masses.

# CHAPTER 5

# CONCLUSIONS

The control of flutter of a wing box using piezoelectric actuators has been presented. The free vibration frequencies have been changed by the piezoelectric actuators in order to increase the flutter speed due to changed mode coalescence. The frequencies and modes can be changed by changing the design variables or using piezoelectric actuators. The examples have indicated that the required flutter velocity of a wing box can be met by the addition of piezoelectric actuators in addition to changing design variables. The examples further demonstrated that, for the cases and parameters chosen, noticeable reduction in weight of the wing boxes can be achieved by the addition of piezoelectric actuators.

## Structural Dynamics and Control Summary

The trends of natural frequencies and flutter velocities suggest that changing the free vibration frequencies using piezoelectric actuators is similar to changing the skin, web, and rib thicknesses and the spar cap and vertical post cross sectional areas. Increasing the frequency of the torsional type modes by piezoelectric actuation is comparable to decreasing the spar cap and vertical post cross sectional areas or to increasing the skin, web, and rib thicknesses. Decreasing the frequency of the torsional type modes by piezoelectric actuation is comparable to increasing the spar cap and vertical post cross sectional areas or decreasing the skin, web, and rib thicknesses.

For several cases, a savings in the weight of the wing box has been gained. The most notable of these examples are the comparisons of increasing spar cap and vertical post area with increasing the free vibration frequencies to meet the desired flutter speed. Flutter requirements are met by taking advantage of the characteristics of the flutter curves owing to the change in mode coalescence due to frequency crossing and mode switching.

## Recommendations

This study was limited in several ways. The most obvious limitation is the selection of only one wing box configuration on which to perform analyses. The wing box was further confined to only two variables of interest: cross sectional area of spar caps and vertical posts, and thicknesses of skins, webs, and ribs. The logical next step is to perform an optimization study for a wider range of wing box designs so as to draw more concrete conclusions on and provide more insight to the concept of using piezoelectric actuators.

The aerodynamic and flutter analyses were restricted to a first order high Mach number approximation to the linear potential flow theory with damping terms neglected. Adding the damping term to simulate the quasi-steady case, or the addition of unsteady aerodynamic terms could be desirable.

The control of the wing box was limited to changing the free vibration frequencies using a single feedback variable. It is a logical next step to apply multi-input multi-output control to change the free vibration characteristics and to increase the flutter speed while achieving weight savings.

# LIST OF REFERENCES

# LIST OF REFERENCES


1. Zeiler, T. A., and Weisshaar, T. A., "Integrated Aeroservoelastic Tailoring of Lifting Surfaces," *Journal of Aircraft*, Vol. 25, No. 1, 1988, pp. 76-83.

2. Karpel, M., "Sensitivity Derivatives of Flutter Characteristics and Stability Margins for Aeroservoelastic Design," *Journal of Aircraft*, Vol. 27, No. 4, 1990, pp. 368-375.

3. Noll, T. E., "Aeroservoelasticity," AIAA Paper 90-1073-CP, April 1990.

4. Wada, B. K., Fanson, J. I., and Crawley, E. F., "Adaptive Structures," *Mechanical Engineering*, Vol. 112, No. 11, 1990, pp. 41-46.

5. Stevens, T., "Structures Get Smart, Part I," *Materials Engineering*, Vol. 108, No. 10, 1991, pp. 18-20.

6. Stevens, T., "Structures Get Smart, Part II," *Materials Engineering*, Vol. 108, No. 11, 1991, pp. 26-28.

7. Wada, B. K., "Adaptive Structures: An Overview," *Journal of Spacecraft*, Vol. 20, No. 3, 1990, pp. 330-337.

8. Jaffe, B., Cook, W. R., and Jaffe, H., "Historical Introduction," *Piezoelectric Ceramics*, Academic Press Limited, India, 1971, pp. 1-5.

9. Mason, W. P., "Piezoelectricity, It's History and Applications," *Journal of Acoustics Society of America*, Vol. 70, No. 6, 1981, pp. 1561-1566.

10. Barrett, R., "Modeling Techniques and Design Principles of a Low Aspect Ratio Active Aeroservoelastic Wing," *Smart Structures and Materials 1993: Smart Structures and Intelligent Systems*, Proc. SPIE Vol. 1917, pp. 107-118.

11. Abdul-Wahed, M. N., and Weisshaar, T. A., "Active Tailoring of Adaptive Lifting Surfaces for Aeroelastic Applications," *Smart Structures and Materials 1993: Smart Structures and Intelligent Systems*, Proc. SPIE Vol. 1917, pp. 72-83.

12. de Luis, J., and Crawley, E. F., "Experimental Results of Active Control on a Prototype Intelligent Structure," AIAA Paper 90-1163-CP, April 1990.

13. Ehlers, S. M., and Weisshaar, T. A., "Static Aeroelastic Behavior of an Adaptive Laminated Piezoelectric Composite Wing," AIAA Paper 90-1078-CP, April 1990.

14. Lazarus, K. B., Crawley, E. F., and Bohlmann, J. D., "Static Aeroelastic Control Using Strain Actuated Adaptive Structures," *Proceedings of the First Joint U. S./Japan Conference on Adaptive Structures*, Maui, Hawaii, October 1990.

15. Lazarus, K. B., Crawley, E. F., and Lin, C. Y., "Fundamental Mechanisms of Aeroelastic Control with Control Reversal and Strain Actuation," AIAA Paper 91-0985-CP, April 1991.

16. Venkayya, V. B., and Tischler, V. A., "'ANALYZE' Analysis of Aerospace Structures with Membrane Elements," Air Force Flight Dynamics Lab., AFFDL-TR-78-170, December 1978.

17. Striz, A. G., and Venkayya, V. B., "Influence of Structural and Aerodynamic Modeling on Flutter Analysis," AIAA Paper 90-0954-CP, April 1990.

18. Rudisill, C. S., and Bhatia, K. G., "Optimization of Complex Structures to Satisfy Flutter Requirements," *AIAA Journal*, Vol. 9, No. 8, 1971, pp. 1487-1491.

19. Rudisill, C. S., and Bhatia, K. G., "Second Derivatives of the Flutter Velocity and the Optimization of Aircraft Structures," *AIAA Journal*, Vol. 10, No. 12, 1972, pp. 1569-1572.

20. Bowman, K. B.; Grandhi, R. V.; and Eastep, F. E., "Structural Optimization of Lifting Surfaces with Divergence and Control Reversal Constraint," *Structural Optimization,* Vol. 1, 1989, pp. 153-161.

21. Megson, T. H. G., "Stress Analysis of Aircraft Components," *Aircraft Structures*, 2nd ed., Halsted Press, New York, 1990, pp. 313-389.

22. Carter, R. E., "Transducer Elements," *Piezo Systems Product Catalog*, Piezo Systems, Inc., Cambridge, Massachusetts, 1990.

23. Yang, T. Y., "Initial and Thermal Forces in Truss Structures," *Finite Element Structural Analysis*, Prentice Hall, Inc., New Jersey, 1986, pp. 90-91.

24. Skelton, R. E., "Pole Assignment," *Dynamic Systems Control*, John Wiley and Sons, Inc., U.S.A., 1988, pp. 318-321.

25. Hemmig, F. G., Venkayya, V. B., Eastep, F. E., "Flutter Speed Degradation of Damaged, Optimized Flight Vehicles," AIAA Paper 79-0795, April 1979.

26. Bisplinghoff, R. L., Ashley, H., and Halfman, R. L., "Introduction to Aeroelasticity," *Aeroelasticity*, John Wiley and Sons, New York, 1955, pp. 1-14.